www.lajss.org
Latin American Journal of Solids and Structures 5 (2008)319–363

Chaotic vibrations in flexible multi-layered Bernoulli-Euler and Timoshenko type beams

J. Awrejcewicz[1,*], A. V. Krysko[2], M.V. Zhigalov[2], O.A. Saltykova[2] and V. A. Krysko[2]

[1] Technical University of Lodz, Department of Automatics and Biomechanics,
1/15 Stefanowskiego St., 90-924 Lodz, Poland
[2] Department of Mathematics, Saratov University, 410054 Saratov, Russia

Abstract

Numerical investigations of transversally driven beams are carried out versus control parameters, i.e. amplitude and frequency of an external loading for a series of boundary conditions and for two kinematical beam models of Euler-Bernoulli and Timoshenko types. Novel stiff stability beam loss is detected and studied. Reliability of the obtained results is verified via FEM (Finite Element Method) and FDM (Finite Difference Method). Transitional and chaotic phenomena exhibited by flexible Euler-Bernoulli beams subjected to an impact action of a one-degree of freedom body with a given mass and velocity are analyzed. It has been shown, among the others, that inclusion of transversal shears and rotation inertia essentially influences nonlinear dynamics of the studied beams subjected to transversal and sign-changeable load actions.

1 Introduction

Recently, an interest in the investigation of regular and chaotic dynamics of continuous systems has been observed. However, rather simple modeling is applied resulting in a study of 1DOF or 2DOF lumped systems yielded by one or two modes approximation and the application of Bubnov-Galerkin method (BGM) [12]. For instance, in references [7, 8] BGM is applied to study nonlinear vibrations of the Bernoulli-Euler beams with one mode approximation taking into account geometric nonlinearities. However, there are many examples which show that the application of more modes yields even qualitatively different results (see, for instance, results reported in [11]). It is well known that validity of the results plays a crucial role, particularly in the analysis of chaotic vibrations of such construction members as plates and shells [2–6]. Among a series of works devoted to the analysis of beam chaotic vibrations, important results are obtained in [10], where nonlinear behavior (including chaos) of an elastic beam with large deflections is studied, and also in reference [14], where global bifurcations and chaotic dynamics of a console beam subjected to axial and transversal harmonic loading are reported.

*Corresp. author Email: awrejcew@p.lodz.pl Received 5 May 2008; In revised form 28 July 2008

In this work new theoretical and numerical results devoted to vibrations of flexible Bernoulli-Euler and Timoshenko type beams are presented.

2 Mathematical models of flexible multi-layered beams

2.1 Problem formulation

We are focused on the investigation of multi-layered beam being a 2D object in space R^2 with rectangular co-ordinates introduced in the following way. In the beam body a certain arbitrary reference curve $z = 0$ is fixed; the axis $0X$ goes along main curvature of the reference curve, whereas the axis $0Z$ is directed to the reference curvature center. In the given coordinates the beam (as a 2D object Ω) is defined as: $\Omega = \{(x, z) / (x) \in [0, a], \delta_0 - \Delta \leq z \leq \delta_{n+m} - \Delta\}$, where $[0, a]$ defines a straight beam line; $\delta_{n+m} - \delta_0 = 2h$ —constant beam thickness; $z = \delta_0 - \Delta$ —lower beam face; $z = \delta_{n+m} - \Delta$ —upper beam face; Δ —beam thickness measured from upper beam face surface to the surface $z = 0$.

2.1.1 Fundamental hypotheses of mathematical beam models

In order to establish the mathematical beam models the following assumptions regarding beam geometry, material properties, beam layers and beam exploitation conditions are introduced.

1) We denote by δ_i, $i = 0, n + m$, thickness of the i-th beam layer; m —number of beam layers regarding the layer containing the surface $z = 0$; n —number of remaining layers. Interval of $z \in (\delta_0 - \Delta, \delta_{n+m} - \Delta)$ is partitioned into intervals regarding z within one layer $(\delta_i - \Delta, \delta_{i+1} - \Delta)$.

2) We assume that normal stresses $\sigma_{zz} = 0$ are small in comparison with other stresses in the beam governing equations.

3) Piece-wise homogeneous beam members (layers) of constant thickness are studied, and therefore the beam is a composition of the layers having different stiffness and being arbitrarily situated regarding the reference surface $z = 0$. If the layers are orthotropic, then in each of them there is an elasticity symmetry plane parallel to a plane tangent to the reference surface, whereas two remaining planes are perpendicular to the axes $0X$.

4) Deformable beam state is studied assuming that deflections of the reference surface are of the order of beam thickness.

5) We denote by $u = u(x, t)$, $W = W(x, t)$ components of the displacement vector of the surface $z = 0$; $u^z = u(x, z, t)$, and $W^z = W(x, z, t)$ denotes displacements of an arbitrary beam point.

6) Let the loading vector on external beam surfaces have the form: $q^+ = q$; $\bar{q} = 0$.

7) Only thin beams are analyzed, and owing to reference [1], the beam arbitrary layer deformation is as follows:

$$e_{xx}^z = \frac{\partial u^z}{\partial x} + \frac{1}{2}\left(\frac{\partial W^z}{\partial x}\right), \quad e_{xz}^z = \frac{\partial u^z}{\partial z} + \frac{\partial W^z}{\partial x}. \tag{1.1}$$

8) A transition from 2D theory of multilayered beams to 1D theory is carried out by introducing a series of static and kinematical hypotheses.

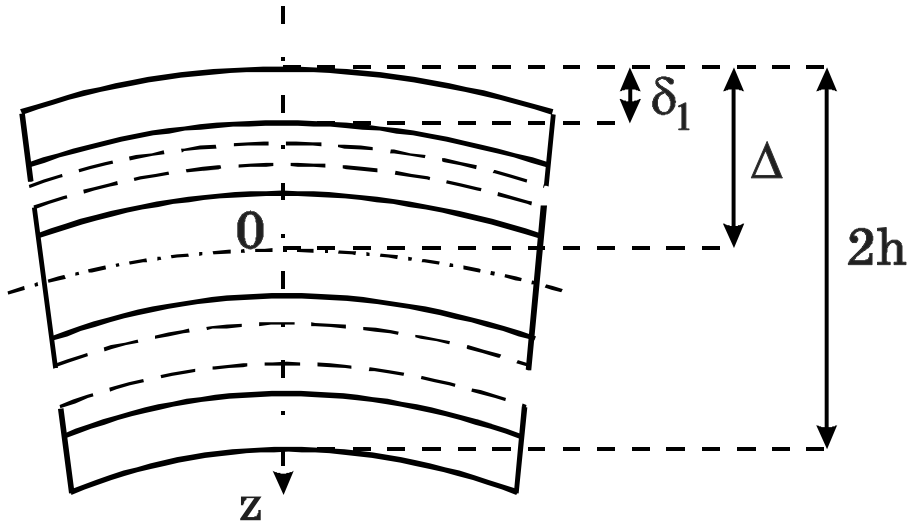

Figure 1.1: Studied beam deformation and position of layers

2.2 The Bernoulli-Euler model

We assume that tangential displacements u^z, W^z are distributed along the layer thickness within the following linear rule:

$$u^z = u - z\frac{\partial W}{\partial x}, W^z = W. \tag{1.2}$$

Hence, taking into account (1.2), equation (1.1) gives

$$e_{xx}^z = \frac{\partial u}{\partial x} + \frac{1}{2}\left(\frac{\partial W}{\partial x}\right)^2 - z\frac{\partial^2 W}{\partial x^2}. \tag{1.3}$$

Let us denote by ε_{11} tangential deformations of the middle surface

$$\varepsilon_{11} = \frac{\partial u}{\partial x} + \frac{1}{2}\left(\frac{\partial W}{\partial x}\right)^2, \tag{1.4}$$

then formulas governing deformations of each layer can be presented in the form of linear series regarding z:

$$e^z_{xx} = \varepsilon_{11} - z\frac{\partial^2 W}{\partial x^2}, z \in (\delta_i - \Delta, \delta_{i+1} - \Delta)\,. \tag{1.5}$$

Hooke's law applied to each of the i-th layer has the following form:

$$e^i_{xx} = \frac{1}{E^i_1}\sigma^i_{xx} - \frac{v^i_{13}}{E^i_1}\sigma^i_{zz}; e^i_{zz} = \frac{-v^i_{31}}{E^i_3}\sigma^i_{xx} + \frac{1}{E^i_3}\sigma^i_{zz}. \tag{1.6}$$

Solving system (1.6) with respect to σ^i_{xx}, σ^i_{zz} yields:

$$\sigma^i_{xx} = \frac{E^i_1}{\bar{\Delta}^i}e^i_{xx} + \frac{E^i_1 v^i_{31}}{\bar{\Delta}^i}e^i_{zz}, \sigma^i_{zz} = \frac{E^i_3 v^i_{13}}{\bar{\Delta}^i}e^i_{xx} + \frac{E^i_3}{\bar{\Delta}^i}e^i_{zz}, \tag{1.7}$$

where E^i_1, E^i_3 are the elasticity modules, and v^i_{13}, v^i_{31} are Poisson's coefficients in the i-th layer, whereas $\bar{\Delta}^i = 1 - v^i_{31}v^i_{13}$.

For chosen orthotropic properties of the material layers the following formula holds

$$E^i_3 v^i_{13} = E^i_1 v^i_{31}, \tag{1.8}$$

which means that $E^i_1 = E^i_3 v^i_{13}/v^i_{31}$.

Owing to the static hypothesis $\sigma_{zz} = 0$, the second equation of (1.7) yields the formula for deformation ε^i_{zz}, which is then substituted to the first relation of (1.7) taking into account (1.8). As a result one obtains:

$$\sigma^i_{xx} = E^i_1 e^i_{xx}. \tag{1.9}$$

Stresses in each beam layer are defined as follows

$$\sigma^i_{xx} = E^i_1\varepsilon_{11} - zE^i_1\frac{\partial^2 W}{\partial x^2}. \tag{1.10}$$

Next, we derive a beam dynamics equation as well as the associated boundary conditions from the point of view of energy distribution analysis.

We consider the process of beam motion on the interval of time instants t_0 and t_1. For this time interval various trajectories of the system points between initial and final states are compared. Real trajectories differ from other possible trajectories (allowed by constraints) by satisfying the following condition:

$$\int_{t_0}^{t_1}\left(\delta K - \delta\Pi + \delta' A\right)dt = 0, \tag{1.11}$$

where K denotes the system kinetic energy, Π is the system potential energy, and $\delta' A$ is the sum of elementary works of the external forces.

In this case, when all forces acting on the system have a potential, equation (1.11) takes the following form

$$\delta S = \delta \int_{t_0}^{t_1} (K - \Pi)\, dt = 0, \tag{1.12}$$

where $S = \int_{t_0}^{t_1} (K - \Pi)\, dt$ is the Hamilton action. The last equation presents the well known Hamilton-Ostrogradskiy principle. In (1.12) $\Pi = \Pi_C + \Pi_i$, where Π_C is the deformation energy of the middle surface, and Π_i is the energy of the bending deformation.

Proceeding in an analogous way as in the case of one-layered beam, we denote by T_{11} internal stresses in the middle beam line, by Q_1 the shearing forces, and by M_{11} the bending moment:

$$T_{11} = \sum_{i=0}^{k} \int_{\alpha_i}^{\alpha_{i+1}} {\sigma_{xx}}^i dz, M_{11} = \sum_{i=0}^{k} \int_{\alpha_i}^{\alpha_{i+1}} {\sigma_{xx}}^i z dz, \tag{1.13}$$

where $n + m - 1 = k$, $\delta_i - \Delta = \alpha_i$, $\delta_{i+1} - \Delta = \alpha_{i+1}$.

Let us first define variation of the potential beam energy $\delta\Pi$. Observe that energy Π_C is

$$\Pi_C = \frac{1}{2} \int T_{11} \varepsilon_{11} dx, \tag{1.14}$$

and energy of bending has the following form

$$\Pi_i = \frac{1}{2} \int M_{11} \left(-\frac{\partial^2 W}{\partial x^2} \right) dx. \tag{1.15}$$

Kinetic beam energy is:

$$K = \frac{1}{2} \frac{\gamma}{g} (2h_0) \int \left[\left(\frac{\partial u}{\partial t} \right)^2 + \left(\frac{\partial W}{\partial t} \right)^2 \right] dx. \tag{1.16}$$

Elementary work of external forces has the following form

$$\delta' A = \int (P_x \delta u + q \delta W)\, dx, \tag{1.17}$$

where P_x denotes normal load and q denotes transversal load. After some transformations the following equations of motion are obtained:

$$\frac{\partial T_{11}}{\partial x} + P_x - \frac{\gamma}{g} (2h_0) \frac{\partial^2 u}{\partial t^2} = 0,$$

$$\frac{\partial^2 M_{11}}{\partial x^2} + \frac{\partial}{\partial x} \left(T_{11} \frac{\partial W}{\partial x} \right) + q - \frac{\gamma}{g} (2h_0) \frac{\partial^2 W}{\partial t^2} = 0. \tag{1.18}$$

Substituting formulas for T_{11} and M_{11} governed by (1.4) and (1.5) into (1.18) one gets

$$T_{11} = \left(\sum_{i=0}^{k} \int_{\alpha_i}^{\alpha_{i+1}} E_1^i dz \right) \varepsilon_{11} - \left(\sum_{i=0}^{k} \int_{\alpha_i}^{\alpha_{i+1}} E_1^i z dz \right) \frac{\partial^2 W}{\partial x^2},$$

$$M_{11} = \left(\sum_{i=0}^{k} \int_{\alpha_i}^{\alpha_{i+1}} E_1^i z dz \right) \varepsilon_{11} - \left(\sum_{i=0}^{k} \int_{\alpha_i}^{\alpha_{i+1}} E_1^i z^2 dz \right) \frac{\partial^2 W}{\partial x^2} \tag{1.19}$$

Introducing the following notation

$$C_{11} = \sum_{i=0}^{k} \int_{\alpha_i}^{\alpha_{i+1}} E_1^i dz, K_{11} = \sum_{i=0}^{k} \int_{\alpha_i}^{\alpha_{i+1}} E_1^i z dz, D_{11} = \sum_{i=0}^{k} \int_{\alpha_i}^{\alpha_{i+1}} E_1^i z^2 dz \tag{1.20}$$

one gets

$$T_{11} = C_{11}\varepsilon_{11} - K_{11}\frac{\partial^2 W}{\partial x^2}, M_{11} = K_{11}\varepsilon_{11} - D_{11}\frac{\partial^2 W}{\partial x^2}. \tag{1.21}$$

Substituting formulas of (1.21) into (1.18) and taking into account (1.4) we get:

$$\frac{\partial C_{11}}{\partial x}\left[\frac{\partial u}{\partial x} + \frac{1}{2}\left(\frac{\partial W}{\partial x}\right)^2\right] + C_{11}\frac{\partial}{\partial x}\left[\frac{\partial u}{\partial x} + \frac{1}{2}\left(\frac{\partial W}{\partial x}\right)^2\right] -$$

$$-\frac{\partial K_{11}}{\partial x}\frac{\partial^2 W}{\partial x^2} - K_{11}\frac{\partial^3 W}{\partial x^3} + P_x - \frac{\gamma}{g}(2h_0)\frac{\partial^2 u}{\partial t^2} = 0,$$

$$\frac{\partial^2}{\partial x^2}\left\{K_{11}\left[\frac{\partial u}{\partial x} + \frac{1}{2}\left(\frac{\partial W^2}{\partial x}\right)^2\right] - D_{11}\frac{\partial^2 W}{\partial x^2}\right\} +$$

$$+\frac{\partial}{\partial x}\left\{C_{11}\left[\frac{\partial u}{\partial x} + \frac{1}{2}\left(\frac{\partial W^2}{\partial x}\right)^2\right] - K_{11}\frac{\partial^2 W}{\partial x^2}\right\}\frac{\partial W}{\partial x} +$$

$$+q - \frac{\gamma}{g}(2h_0)\frac{\partial^2 W}{\partial t^2} = 0. \tag{1.22}$$

In the case of one-layered and homogeneous beam of constant cross section, equations (1.22) take the form

$$E(2h_0)\left\{\frac{\partial^2 u}{\partial x^2} + L_3(W,W) - (2h_0)\frac{\gamma}{g}\frac{\partial^2 u}{\partial t^2}\right\} = 0,$$

$$E(2h_0)\left\{L_1(u,W) + L_2(W,W) - \frac{(2h_0)^2}{12}\frac{\partial^4 W}{\partial x^4}\right\} + q - (2h_0)\frac{\gamma}{g}\frac{\partial^2 u}{\partial t^2} = 0, \tag{1.23}$$

where

$$L_1(u,W) = \frac{\partial^2 u}{\partial x^2}\frac{\partial W}{\partial x} + \frac{\partial u}{\partial x}\frac{\partial^2 W}{\partial x^2},$$

$$L_2(W,W) = \frac{3}{2}\frac{\partial^2 W}{\partial x^2}\left(\frac{\partial W}{\partial x}\right)^2,$$
$$L_3(W,W) = \frac{\partial^2 W}{\partial x^2}\frac{\partial W}{\partial x} \tag{1.24}$$

are nonlinear operators.

System (1.23) should be supplemented by one of the following boundary conditions:

1. Clamping
$$w = 0; u = 0; \frac{\partial w}{\partial x} = 0; \tag{1.25}$$

2. Simple support
$$w = 0; u = 0; M_x = 0; \tag{1.26}$$

3. Free edge
$$M_x = 0; N_x = 0; Q_x = 0; \tag{1.27}$$

and the following initial condition

$$w_{|t=0} = \dot{w}_{|t=0} = u_{|t=0} = \dot{u}_{|t=0} = 0. \tag{1.28}$$

2.3 The Timoshenko beam model

We assume that tangential displacements u^z, W^z are distributed along thickness of the layers package via a linear rule, i.e.

$$u^z = u + z\gamma_x, W^z = W, \tag{1.29}$$

where $\gamma_x = \gamma_x(x)$ is the angle of normal rotation to the surface $z = 0$ generated by deformation in the plane $X0Z$. Then from (1.1) and taking into account (1.29) one gets

$$e^z_{xx} = \frac{\partial u}{\partial x} + \frac{1}{2}\left(\frac{\partial W}{\partial x}\right)^2 + z\frac{\partial \gamma_x}{\partial x}; e^z_{xz} = \gamma_x + \frac{\partial W}{\partial x}. \tag{1.30}$$

Now, if we denote tangential deformations of the middle beam line by ε_{11} using the formula

$$\varepsilon_{11} = \frac{\partial u}{\partial x} + \frac{1}{2}\left(\frac{\partial W}{\partial x}\right)^2, \tag{1.31}$$

and bending deformations by $H_{11} = \frac{\partial \gamma_x}{\partial x}$, shear deformations by $\varepsilon_{13} = \gamma_x + \frac{\partial W}{\partial x}$, then formulas governing each beam layer deformation can be presented by the linear formula regarding z:

$$e^z_{xx} = \varepsilon_{11} + zH_{11}; e^z_{xz} = \varepsilon_{13}; z \in (\delta_i - \Delta, \delta_{i+1} - \Delta). \tag{1.32}$$

Hooke's law for each i-th orthotropic layer is

$$e_{xx}^i = \frac{1}{E_1^i}\sigma_{xx}^i - \frac{v_{13}^i}{E_1^i}\sigma_{zz}^i; e_{zz}^i = \frac{-v_{31}^i}{E_3^i}\sigma_{xx}^i + \frac{1}{E_3^i}\sigma_{zz}^i; e_{xz}^i = \frac{\sigma_{xz}^i}{G_{13}^i}, \tag{1.33}$$

and hence one gets

$$\sigma_{xx}^i = \frac{E_1^i}{\bar{\Delta}^i}e_{xx}^i + \frac{E_1^i\left(v_{31}^i\right)}{\bar{\Delta}^i}e_{zz}^i; \sigma_{zz}^i = \frac{E_3^i\left(v_{13}^i\right)}{\bar{\Delta}^i}e_{xx}^i + \frac{E_3^i}{\bar{\Delta}^i}e_{zz}^i; \sigma_{xz}^i = G_{13}^i e_{xz}^i, \tag{1.34}$$

where E_1^i, E_3^i are the elasticity modules; v_{13}^i, v_{31}^i are Poisson's coefficients; G_{13}^i is the shear modulus in the i-th layer, and $\bar{\Delta}^i = 1 - v_{31}^i v_{13}^i$. For a chosen type of material othotropy the following relations hold

$$E_3^i v_{13}^i = E_1^i v_{31}^i, \tag{1.35}$$

which yields $E_1^i = \frac{E_3^i v_{13}^i}{v_{31}^i}$.

Taking into account the static hypothesis $\sigma_{zz}^i = 0$, a formula for deformation e_{zz}^i is found and then it is substituted into first two relations of (1.34). Hence, stress tensor components in each beam layer have the following forms:

$$\sigma_{xx}^i = E_1^i e_{xx}^i, \sigma_{xz}^i = G_{13}^i e_{xz}^i. \tag{1.36}$$

Denoting

$$\varphi_1^i = E_1^i, \varphi_2^i = 0, \tag{1.37}$$

and taking into account (1.32), the following formulas describing stresses in each beam layer are derived

$$\sigma_{xx}^i = \varphi_1^i \varepsilon_{11} + z\varphi_1^i H_{11}, \sigma_{xz}^i = G_{13}^i \varepsilon_{13}. \tag{1.38}$$

Let us denote $n + m - 1 = k$, $\delta_i - \Delta = a_i$, $\delta_{i+1} - \Delta = a_{i+1}$, and in the way analogous to that of one layer beam we denote internal stresses by T_{11}, shearing forces by Q_1, and bending moment of the form by M_{11}

$$T_{11} = \sum_{t=0}^{k}\int_{a_i}^{a_{i+1}} \sigma_{xx}^t dz; Q_1 = \sum_{i=0}^{k}\int_{a_i}^{a_{i+1}} \sigma_{xz}^1 dz; M_{11} = \sum_{t=0}^{k}\int_{a_i}^{a_{i+1}} \sigma_{xx}^1 \cdot z dz \tag{1.39}$$

respectively, and then

$$\delta V = \int \left(T_{11}\delta\varepsilon_{11}\right) dX + \int \left(M_{11}\delta H_{11}\right) dX + \int \left(Q_1 \delta\varepsilon_{13}\right) dX. \tag{1.40}$$

Substituting into (1.34) the formulas for σ_{xx}^i and σ_{xz}^i given by (1.40), one gets

$$T_{11} = \left(\sum_{i=0}^{k}\int_{\alpha_i}^{\alpha_{i+1}} \varphi_1^i dz\right)\varepsilon_{11} + \left(\sum_{i=0}^{k}\int_{\alpha_i}^{\alpha_{i+1}} \varphi_1^i z dz\right) H_{11},$$

$$Q_1 = \left(\sum_{i=0}^{k} \int_{\alpha_i}^{\alpha_{i+1}} G_{13}^i dz \right) \varepsilon_{13},$$

$$M_{11} = \left(\sum_{i=0}^{k} \int_{\alpha_i}^{\alpha_{i+1}} \varphi_1^i z dz \right) \varepsilon_{11} + \left(\sum_{i=0}^{k} \int_{\alpha_i}^{\alpha_{i+1}} \varphi_1^i z^2 dz \right) H_{11}. \tag{1.41}$$

Coefficients of series (1.41) have the following form

$$C_{11} = \sum_{i=0}^{k} \int_{a_i}^{a_{i+1}} \varphi_j^i dz; K_{11} = \sum_{i=0}^{k} \int_{a_i}^{a_{i+1}} \varphi_j^i \cdot z dz;$$

$$D_{11} = \sum_{i=0}^{k} \int_{a_i}^{a_{i+1}} \varphi_j^i \cdot z^2 dz; A_{44} = \sum_{i=0}^{k} \int_{a_i}^{a_{i+1}} G_{13}^i dz; j = 1, 2, l = 2, 1, \tag{1.42}$$

and therefore formula (1.41) takes the following form

$$T_{11} = C_{11}\varepsilon_{11} + K_{11}H_{11}, Q_1 = A_{44}\varepsilon_{13}, M_{11} = K_{11}\varepsilon_{11} + D_{11}H_{11}. \tag{1.43}$$

Proceeding in the way similar to that of the Euler-Bernoulli kinematical model, the Hamilton-Ostrogradskiy principle takes the following form

$$\delta S = \delta \int_{t_0}^{t_1} (K - \Pi)\, dt = 0, \tag{1.44}$$

where $\Pi = \Pi_C + \Pi_i$.

Energy of the middle surface Π_C is

$$\Pi_C = \frac{1}{2} \int_e T_{11}\varepsilon_{11} dx = \frac{1}{2} \int_e T_{11} \left[\frac{\partial U}{\partial x} + \frac{1}{2} \left(\frac{\partial W}{\partial x} \right)^2 \right] dx, \tag{1.45}$$

and bending energy Π_i is given in the form

$$\Pi_i = \frac{1}{2} \int_e \left[M_{11}H_{11} + Q_{11} \left(\gamma_x + \frac{\partial W}{\partial x} \right) \right] dx, \tag{1.46}$$

whereas the kinetic energy is

$$K = \frac{1}{2} \frac{\gamma}{g} 2h_0 \int_e \left[\left(\frac{\partial U}{\partial t} \right)^2 + \left(\frac{\partial W}{\partial t} \right)^2 + b \left(\frac{\partial \gamma_x}{\partial t} \right)^2 \right] dx, \tag{1.47}$$

and finally the work of external forces is as follows

$$\delta' A = \int\limits_e \left(P_{11}\delta U + q\delta W\right) dx, \tag{1.48}$$

where the following abbreviations: $\gamma = \sum\limits_{i=0}^{k} \gamma^i$, $b = \sum\limits_{i=0}^{k} \int\limits_{\alpha_i}^{\alpha_{i+1}} z^2 dz$ are applied in equation (1.47).

Substituting (1.45)-(1.48) into (1.44) and applying variation, the following equilibrium equations are obtained

$$\begin{gathered}
\frac{\partial T_{11}}{\partial x} + P_{xx} - \frac{\gamma}{g}\left(2h_0\right)\frac{\partial^2 u}{\partial t^2} = 0, \\
\frac{\partial Q_{11}}{\partial x} + \frac{\partial}{\partial x}\left(T_{11}\frac{\partial W}{\partial x}\right) + q - \frac{\gamma}{g}\left(2h_0\right)\frac{\partial^2 W}{\partial t^2} = 0, \\
\frac{\partial M_{11}}{\partial x} - Q_{11} - \frac{\gamma}{g} b \frac{\partial^2 \gamma_x}{\partial t^2} = 0.
\end{gathered} \tag{1.49}$$

Substituting (1.43) into (1.49) and taking into account (1.31) gives the following Timoshenko equations regarding displacements

$$\begin{gathered}
\frac{\partial}{\partial x}\left\{C_{11}\left[\frac{\partial u}{\partial x} + \frac{1}{2}\left(\frac{\partial W}{\partial x}\right)^2\right] + K_{11}\frac{\partial \gamma_x}{\partial x}\right\} + P_{xx} - \frac{\gamma}{g}\left(2h_0\right)\frac{\partial^2 u}{\partial t^2} = 0, \\
\frac{\partial}{\partial x}\left[A_{44}\left(\gamma_x + \frac{\partial W}{\partial x}\right)\right] + \frac{\partial}{\partial x}\left\{C_{11}\left[\frac{\partial u}{\partial x} + \frac{1}{2}\left(\frac{\partial W}{\partial x}\right)^2\right]\frac{\partial W}{\partial x} + K_{11}\frac{\partial \gamma_x}{\partial x}\frac{\partial W}{\partial x}\right\} + q - \frac{\gamma}{g}\left(2h_0\right)\frac{\partial^2 W}{\partial t^2} = 0 \\
\frac{\partial}{\partial x}\left\{K_{11}\left[\frac{\partial u}{\partial x} + \frac{1}{2}\left(\frac{\partial W}{\partial x}\right)^2\right] + D_{11}\frac{\partial \gamma_x}{\partial x}\right\} - A_{44}\left(\gamma_x \frac{\partial W}{\partial x}\right) - \frac{\gamma}{g} b \frac{\partial^2 \gamma_x}{\partial t^2} = 0
\end{gathered} \tag{1.50}$$

The system of equations (1.50) requires boundary and initial conditions.

1. Either rotation angle around the normal axis OY or the bending moment is given

$$\gamma_x = \gamma_x^0 \; or \; M_{11} = M_{11}^0. \tag{1.51}$$

2. Either normal displacements of the contour points or the value of external transversal stresses is given

$$W = W^0 \; or \; Q_{11} + T_{11}\frac{\partial W}{\partial x} = Q_{11}^0. \tag{1.52}$$

3. Either displacements of the contour points of the middle surface in x directions or the value of external compression stress are given, i.e.

$$u = u^0 \; or \; T_{11} = T_{11}^0. \tag{1.53}$$

Initial conditions are introduced in the following way

$$w_{|t=0} = u_{|t=0} = \gamma_{|t=0} = 0, \dot{w}_{|t=0} = \dot{u}_{|t=0} = \dot{\gamma}_{|t=0} = 0. \tag{1.54}$$

In the mathematical model built on the Bernoulli-Euler hypothesis, the position of a normal element in the extreme cross section after deformation is governed by four parameters. This means that on each of the contour part four boundary conditions are formulated. In the mathematical model based on the Timoshenko hypothesis a number of the degrees of freedom of a normal element reaches five, since now an independent rotation around axis x is allowed (on the boundary x=const).

If transversal rotation is neglected, i.e. $\frac{\partial \delta W}{\partial x} = -\delta\gamma_x$ holds, then removal of term $\delta\gamma_x$ from the variation equation gives the equations corresponding to the Bernoulli-Euler hypotheses instead of equations (1.50).

3 Numerical investigation of chaotic vibrations of flexible Euler-Bernoulli beams

3.1 Problem formulation

Let us introduce the Cartesian coordinates XOZ (Figure 2.1). A thin elastic beam is studied in the space $\Omega = \left\{x \in [0,a]\,; -h \le z \le h; -\frac{b}{2} \le y \le \frac{b}{2}\right\}$, whose middle surface deformation is $\varepsilon_x = \frac{\partial u}{\partial x} + 1/2\left(\frac{\partial w}{\partial x}\right)^2$, where: $w(x,t)$ is the beam deflection and $u(x,t)$ is the displacement of the middle beam line along axis ox. It is assumed that owing to the Bernoulli-Euler hypothesis a normal to the middle line remains normal after the beam deformation i.e. $\varepsilon_{xx} = \varepsilon_x - z\frac{\partial^2 w}{\partial x^2}$, where ε_x denotes the middle beam line deformation, $N_x = \int\limits_{-h}^{h} \sigma_{xx} dz$ is the longitudinal stress, and $M_x = \int\limits_{-h}^{h} \sigma_{xx} z dz = -\frac{(2h)^3}{12} E \frac{\partial^2 w}{\partial x^2}$ denotes the bending moment [13].

The system of differential equations in displacements, governing the beam motion including energy dissipation, after introduction of the following non-dimensional parameters

$$\bar{w} = \frac{w}{(2h)}, \bar{u} = \frac{ua}{(2h)^2}, \bar{x} = \frac{x}{a}, \lambda = \frac{a}{(2h)}, \bar{q} = q\frac{a^4}{(2h)^4 E},$$
$$\bar{t} = \frac{t}{\tau}, \tau = \frac{a}{c}, c = \sqrt{\frac{Eg}{\gamma}}, \bar{\varepsilon_i} = \varepsilon_i \frac{a}{c}, i = 1,2, \tag{2.1}$$

is written in the following non-dimensional form

$$\begin{cases} \frac{\partial^2 u}{\partial x^2} + L_3(w,w) - \frac{\partial^2 u}{\partial t^2} - \varepsilon_2 \frac{\partial u}{\partial t} = 0, \\ \frac{1}{\lambda^2}\left\{L_2(w,w) + L_1(u,w) - \frac{1}{12}\frac{\partial^4 w}{\partial x^4}\right\} - \frac{\partial^2 w}{\partial t^2} - \varepsilon_1 \frac{\partial w}{\partial t} + q = 0. \end{cases} \tag{2.2}$$

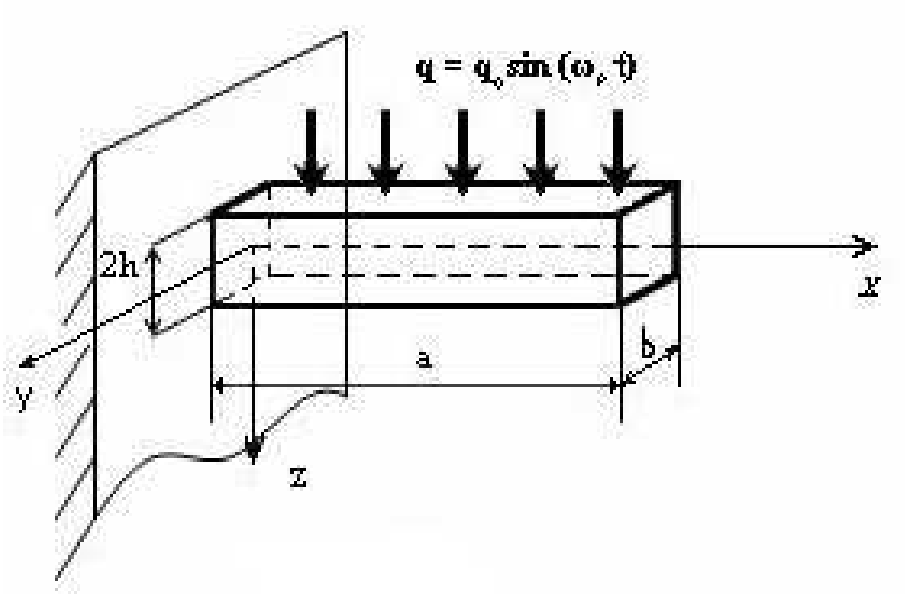

Figure 2.1: Beam geometry and applied load

In the above, bars over non-dimensional parameters are omitted and the following notation is introduced: $L_1(u,w) = \frac{\partial^2 u}{\partial x^2}\frac{\partial w}{\partial x} + \frac{\partial u}{\partial x}\frac{\partial^2 w}{\partial x^2}$, $L_2(w,w) = \frac{3}{2}\frac{\partial^2 w}{\partial x^2}\left(\frac{\partial w}{\partial x}\right)^2$, $L_3(w,w) = \frac{\partial^2 w}{\partial x^2}\frac{\partial w}{\partial x}$; ε_1, ε_2 - damping coefficients; $q = q(x,t)$ - transversal load, E - Young modulus; ρ, γ - density and weight density of the beam, respectively; g - Earth gravitational acceleration.

Equation (2.2) is supplemented by one of the equations on the beam boundaries:

i. "clamping-clamping"

$$w(0,t) = w(a,t) = u(0,t) = u(a,t) = \frac{\partial w(0,t)}{\partial x} = \frac{\partial w(a,t)}{\partial x} = 0; \tag{2.3}$$

ii. "simple support - simple support"

$$w(0,t) = w(a,t) = u(0,t) = u(a,t) = \frac{\partial^2 w(0,t)}{\partial x^2} = \frac{\partial^2 w(a,t)}{\partial x^2} = 0; \tag{2.4}$$

iii. "clamping - simple support"

$$w(0,t) = u(0,t) = w(a,t) = u(a,t) = \frac{\partial w(0,t)}{\partial x} = \frac{\partial^2 w(a,t)}{\partial x^2} = 0; \tag{2.5}$$

iv. "clamping - free edge"

$$w(0,t) = \frac{\partial w(0,t)}{\partial x} = u(0,t) = 0; M_x(a,t) = N_x(a,t) = Q_x(a,t) = 0. \tag{2.6}$$

Additionally, the following initial conditions are added to system (2.2):

$$w(x,t)_{|t=0} = \frac{\partial w(x,t)}{\partial t}_{|t=0} = u(x,t)_{|t=0} = \frac{\partial u(x,t)}{\partial t}_{|t=0} = 0 \tag{2.7}$$

3.2 FDM and PDEs solution

The infinite problem (2.2)-(2.7) will be solved via FDM with the approximation of $O\left(c^2\right)$, and it is reduced to a system of ordinary differential equations (ODEs). In each node of a mesh the following set of ODEs is obtained

$$\begin{cases} L_{1,c}\left(w_i(t), u_i(t)\right) + q_i(t) = \varepsilon_1 \dot{w}_i(t) + \ddot{w}_i(t); \\ L_{2,c}\left(w_i(t), u_i(t)\right) = \varepsilon_2 \dot{u}_i(t) + \ddot{u}_i(t); (i = 0, ..., n), \end{cases} \tag{2.8}$$

where n denotes the partition number regarding a spatial coordinate, c is the computational step regarding spatial coordinate, and $L_{1,c}\left(w_i(t), u_i(t)\right)$, $L_{2,c}\left(w_i(t), u_i(t)\right)$ are the difference operators.

For $i = 1, i = n-1$ in equations (2.8) one needs to find w in the out-of-contour points, which are defined by the boundary conditions. Namely, we have

i. for boundary conditions (2.3): $w_{-i} = w_i$;

ii. for boundary conditions (2.4): $w_{-i} = -w_i$.

Additionally, the system of equations (2.8) is supplemented by the following equations on the boundary, i.e.

iii. Boundary conditions (2.3)-(2.5):

$$w_0 = 0; w_n = 0; u_0 = 0; u_n = 0; \tag{2.9}$$

iv. Boundary conditions (2.6):

$$w_0 = 0; u_0 = 0; M_x = 0; N_x = 0; Q_x = 0 \tag{2.10}$$

Initial conditions for all mentioned boundary conditions have the following difference forms

$$w(x_i)_{|t=0} = 0; u(x_i)_{|t=0} = 0; \dot{w}(x_i)_{|t=0} = 0; \dot{u}(x_i)_{|t=0} = 0, (i = 0, ...n,). \tag{2.11}$$

The obtained system of equations (2.8) with the supplemented boundary and initial conditions (2.9)-(2.11) is solved by the fourth order Runge-Kutta method.

3.3 FEM and PDEs solution

Note that in the field of mechanical structural engineering in spite of the so far applied FDM often FEM and FBE (Finite Boundary Elements) are used. The main idea of application of the mentioned approaches relies on the approximation of a continuous object by a discrete model. The discrete model is obtained on a basis of a set of piece-wise continuous functions defined on a finite set of either subspaces (FDM) or boundaries (MBE).

The methods of formulation of discrete models by FEM are divided into two large groups. The first one uses minimizing conditions of various energy containing functional, whereas the second one relies on the methods of weighted boundary layers including the popular Bubnov-Galerkin method.

In the Bubnov-Galerkin method the functions $w(x)$ and $u(x)$ are approximated as follows

$$\widehat{w} = \sum_{i=1}^{N} \psi_i(x)\, u_i, \widehat{u} = \sum_{i=1}^{N} \varphi_i(x)\, u_i, \tag{2.12}$$

where u_i, w_i are the values of functions $u(x), w(x)$ in the points ($i = \overline{1,N}$) to be found, and $\varphi_i(x)$, $\psi_i(x)$ are the known analytical (testing or form) functions.

Owing to the FEM theory, in order to construct a beam element one has to introduce form functions. The considered beam element has four degrees of freedom $(w_1, w_2, \theta_1, \theta_2)$ and the introduced approximation is associated with the introduction of a cubic polynomial of the form

$$w(x) = a_1 + a_2 x + a_3 x^2 + a_4 x^3, \theta(x) = -\frac{dw}{dx} = -\left(a_2 + 2a_3 x + 3a_4 x^2\right). \tag{2.13}$$

After estimation of the values of constants, the approximating function $w(x)$ has the following form

$$w = \lfloor \mathbf{N}_w \rfloor \{\mathbf{W}\}, \tag{2.14}$$

where $\lfloor \mathbf{N}_w \rfloor = \left(1 - 3\xi^2 + 2\varsigma^3; -l\xi(\xi-1)^2; 3\xi^2 - 2\xi^3; -l\xi\left(\xi^2 - \xi\right)\right)$ is the form matrix; $\{\mathbf{W}\} = (w_1\theta_1 w_2\theta_2)^T$ is the matrix of node displacements; $\xi = x/l$ is the non-dimensional quantity (local coordinate).

Displacement approximation $u(x)$ has the following form

$$u = \lfloor \mathbf{N}_u \rfloor \{\mathbf{U}\}, \tag{2.15}$$

where $\lfloor \mathbf{N}_u \rfloor = (1-\xi; \xi)\{\mathbf{U}\} = (u_1 u_2)^T$.

Applying the Bubnov-Galerkin procedure and taking into account the introduced approximations, the following FEM equations are finally obtained

$$\begin{cases} \left[M_1\left[\ddot{W}(t)\right] + C_1\left[\dot{W}(t)\right] + K_1[W(t)] = F_1(q(t), U(t)), \right. \\ \left. M_2\left[\ddot{U}(t)\right] + C_2\left[\dot{U}(t)\right] + K_2[U(t)] = F_2(W(t)), \right. \end{cases} \tag{2.16}$$

where M_i, C_i, K_i are the mass, damping and stiffness matrices, respectively.

3.4 Reliability of the obtained results

One of the important problems which occur while solving chaotic phenomena in mechanics, is addressing reliability of the obtained results. Since the differential equations governing behavior of the applied mathematical models are essentially nonlinear, analytical solutions cannot be obtained, and hence validity of results of the numerical solution cannot be verified. Therefore, in order to check the computational reliability, a comparison of the results obtained via another numerical technique is highly required. In this work, solutions obtained via FDM and FEM in the Bubnov-Galerkin form are compared. Note, that for either FEM or FDM the partitions are carried out regarding spatial coordinate and time.

In order to investigate convergence regarding the number of partitions of the spatial coordinate applying FDM and FEM, problem (2.6) with the following data: $\varepsilon_1 = 1, \varepsilon_2 = 0$; $\omega_p = 5,1$ –frequency of the driven force with amplitude q_0, and the relative beam length $\lambda = a/2h = 50$, is studied. Time step Δt has been chosen from stability condition of the obtained solutions with respect to the Runge principle, and it is Δt=3.9052·10^{-3}. Convergence regarding spatial coordinates has been verified for $n = 40; 80$ using two different methods (FDM and FEM).

In order to compare numerical results in Tables 2.1 (FDM) and 2.2 (FEM) frequency power spectra and time histories $w\,(t)$ for loading amplitude $q_0 = 100$ (harmonic vibrations regime), as well as for $q_0 = 32200$ (chaotic state), are analyzed.

As it is seen in the tables, the frequency power spectra of a harmonic signal fully coincide for both methods for $n = 40$ and $n = 80$, and the signals differ from each other by 1.5-3%. In the case of chaotic dynamics, the frequency power spectra coincide but they differ regarding frequencies number. The signals differ by 3-5% either for periodic or chaotic vibrations. Therefore, a double increase of the partition number does not lead to essential changes of signals and power spectra in either regular or chaotic states. Next, during our further investigations of the Bernoulli-Euler beams, partitions of $n = 40$ and step $c = 1/40$ are applied.

Table 2.3 presents convergence regarding (FDM, FEM) for the boundary conditions (2.6) and for the parameters as in the previous cases. Table 2.3 shows that for periodic vibrations signals and frequency power spectra obtained via FDM and FEM practically coincide. In the case of chaos signal FDM differs by 2.5-4%. Frequency power spectra for beam chaotic dynamics practically qualitatively coincide, and a difference of 5% is observed in frequencies number. Therefore, owing to analysis of Tables 2.1 - 2.3, one may conclude that the results obtained by FDM and MBM either for harmonic or chaotic regimes are reliable.

In order to investigate non-linear dynamics of the Bernoulli-Euler beams the so called charts of vibration regime depending on two control parameters $\{q_0, \omega_p\}$ are introduced. The charts represent a graphical transformation of the computational results of the investigated dynamical systems. One of the important problems being addressed is that of getting full information of the system dynamics achieved via minimal computational time. The investigations of charts

	Signal $w(t)$	Power spectrum
$q_0 = 100$	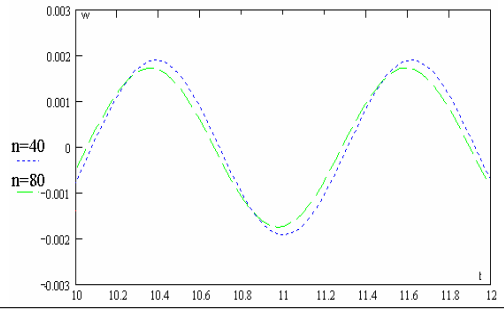	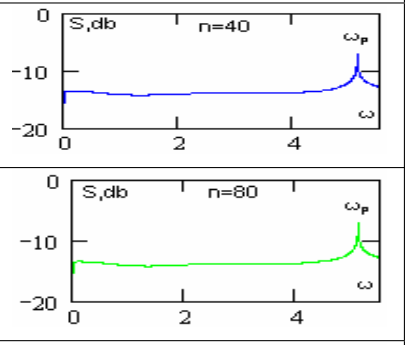
$q_0 = 32200$	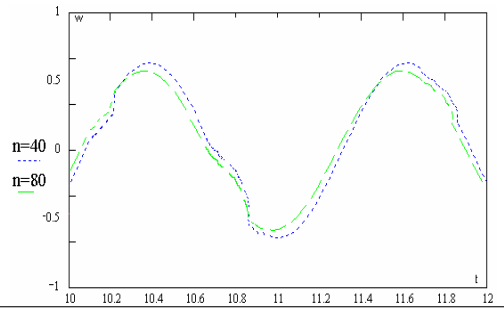	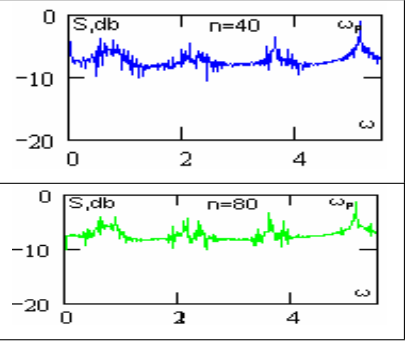

Table 2.1: Signal and frequency power spectra (regular dynamics)

with the resolution of 100×100, 200×200, 300×300, 400×400 reported in reference [9] indicate that the most optimal one is that of the resolution 300×300. However, to construct it one needs to compute and analyze $9 \cdot 10^4 104$ computational variants. Observe that computation with a Celeron 1700 processor using FDM with $n = 40$ requires the computational time of 70 days, whereas for $n = 80$ it needs 140 days. In the case of FEM application the computational time for the same case increases by about 1.5 to 1.7 times.

Table 2.4 gives charts which exhibit the dependence of vibration regimes on two control parameters $\{q_0, \omega_p\}$ for boundary conditions (1.6) and (1.3). Frequency of the excitation load is changed from $\omega_0/2$ (chart I) to $3\omega_0/2$ (chart III), where ω_0 (chart II) is the free beam vibration frequency (for problem 4 - $\omega_0 = 5.1$). Maximum loading amplitude corresponds to the beam deflection $5\,(2h)$. The charts are constructed with the resolution of 300×300.

Analysis of the obtained signals and beam vibration regimes also proves that results are reliable for various forms of vibrations. Note that chaotic zones obtained through FEM are wider regarding frequency in comparison to those obtained via FDM. However, the mentioned zones coincide with respect to amplitude comparison. In the charts clearly periodic, chaotic, and bifurcation zones are presented. For small amplitudes of the excited vibrations one may observe black zones associated with damped system vibrations.

In order to check reliability of the results for different boundary conditions and to save

	Signal $w(t)$	Power spectrum
$q_0 = 100$	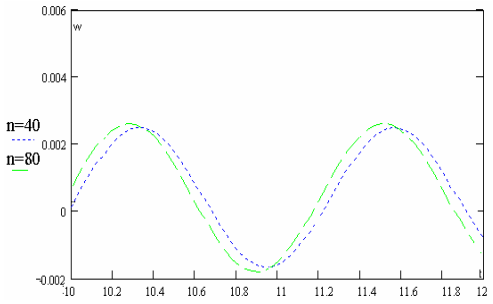	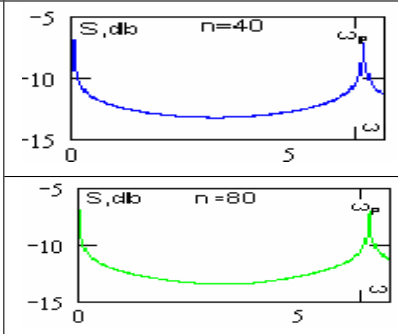
$q_0 = 32200$	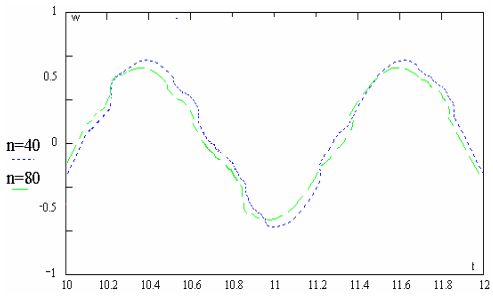	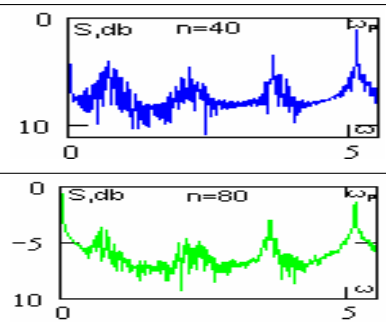

Table 2.2: Signal and frequency power spectra (chaotic dynamics)

computational time, Table 2.5 gives scales associated with vibration type vs. amplitude of excitation $q_0 \in \left[0, 6 \cdot 10^4\right]$ (they are constructed only for one value of ω_p) and the drawings $w_{max}(q_0)$. The stated problems have been solved for the following parameters: $\varepsilon_1 = 1, \varepsilon_2 = 0$, $\lambda = \frac{a}{2h} = 50$, $\omega_p = 6.9$, $n = 40$.

Different boundary conditions essentially influence vibration regime of the investigated system. In the case of clamping-clamping, irrespectively of the numerical approach (FEM or FDM), the system exhibits independent frequency vibrations with zones of bifurcations. A transition to chaos is not observed in this case. In the graph $w_{max}(q_0)$ sudden jumps and discontinuities are not observed. If one considers zones in the case of simple support-simple support, then chaotic zones appear and they are interlaced with bifurcation zones. However, periodic zones are not detected at all in this case.

Observe that the dependence of maximum deflection vs. amplitude of excitation only in the beginning does not have sudden jumps of w_{max} (for $q_0 \in \left[0, 1 \cdot 10^4\right]$). The transition from periodic to chaotic dynamics and vice versa is characterized by a sudden change of w_{max} corresponding to a simultaneous change of the amplitude of vibrations. This observation enables a definition of dynamical stability loss associated with transversal sign-changeable load action.

In the case of asymmetric boundary conditions the transition to chaos occurs for $q_0 \geq 2.5 \cdot 10^4$. For the given boundary conditions periodic vibrations dominate for $q_0 \in \left(1.1 \cdot 10^4, 2.5 \cdot 10^4\right)$.

	Signal $w(t)$	Power spectrum
$q_0 = 100$	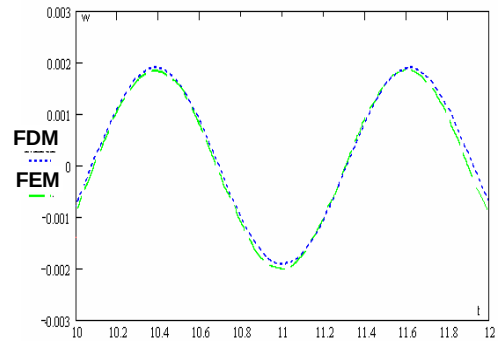	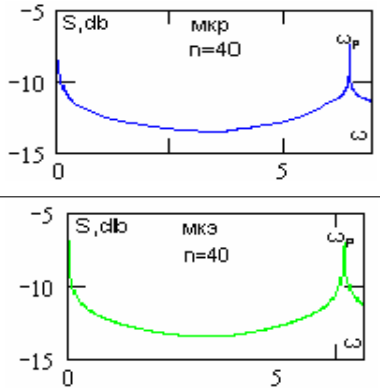
$q_0 = 32200$	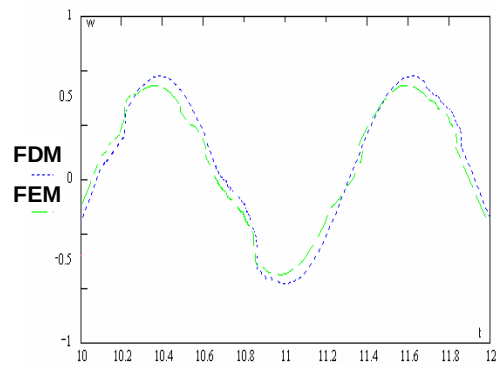	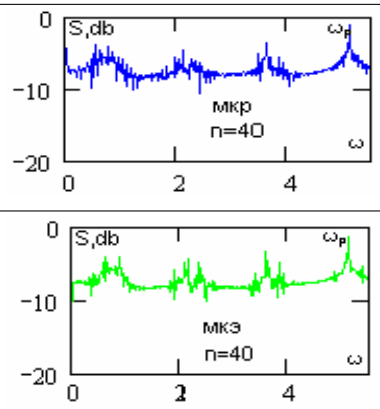

Table 2.3: Convergence of results obtained by FDM and FEM

Observe that in the case of chaos, the dependence $w_{max}(q_0)$ also has discontinuities in spite of sudden jumps of the maximum deflection.

3.5 Chaotic vibrations vs. boundary conditions

We have observed that the obtained results of FEM and FDM are satisfactorily convergent, and since the computational time is essentially lower using FDM computation, therefore the last one is further applied.

We divide the vibration regimes into two classes: class "A" - periodic vibrations with independent frequencies, damped vibrations (engineering-acceptable regimes), and class "B" - bifurcation and chaos, i.e. regimes which are not suitable for construction exploitation.

Table 2.6 gives charts constructed for the Bernoulli-Euler model for boundary conditions (2.3)-(2.5). The beam is transversally driven and the amplitude of excitation is changed in the interval $q_0 \in [0; 32200]$, while the excitation frequency is $\omega_p \in [2.55; 7.65]$.

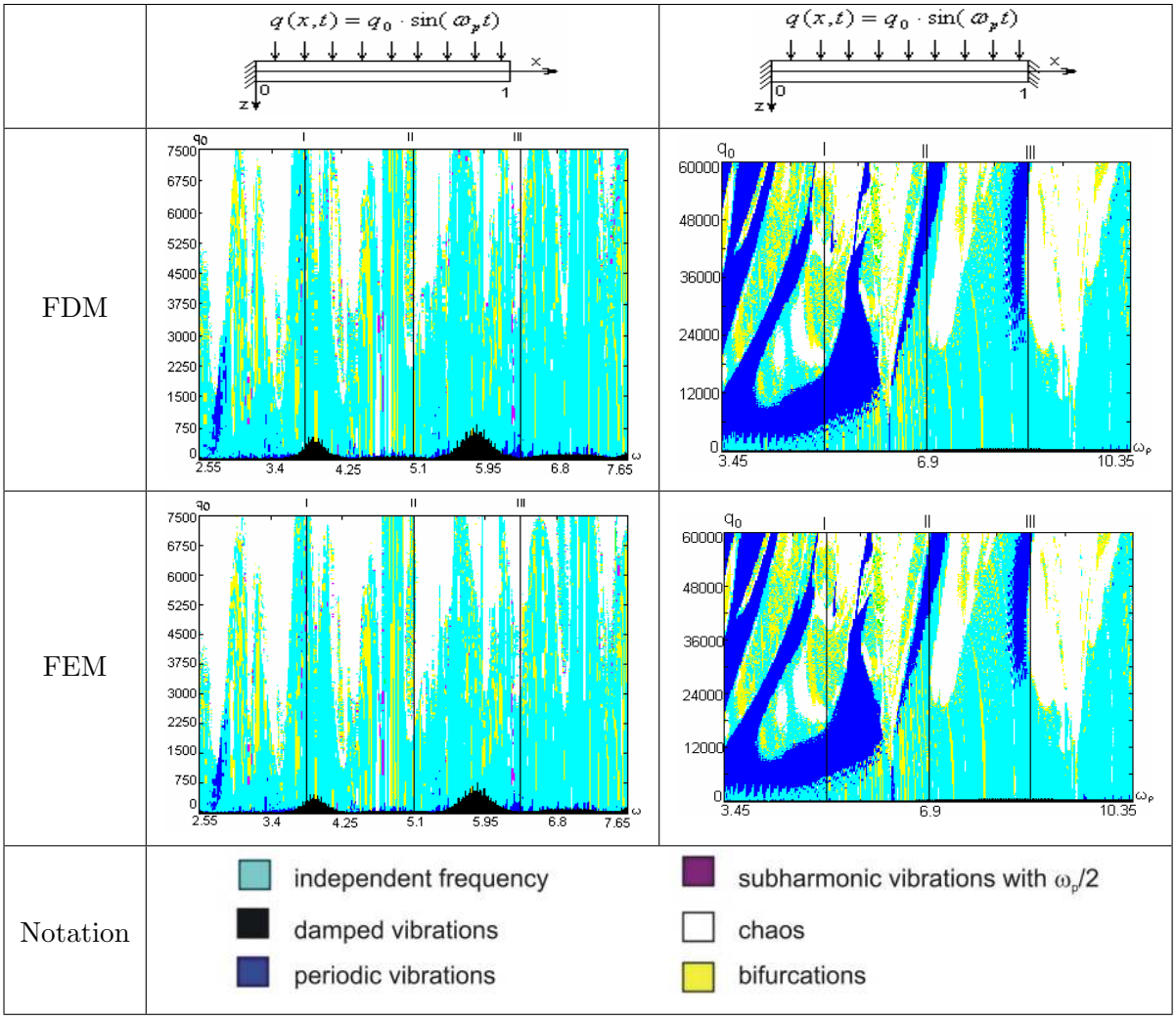

Table 2.4: Vibration type charts obtained by FDM and FEM

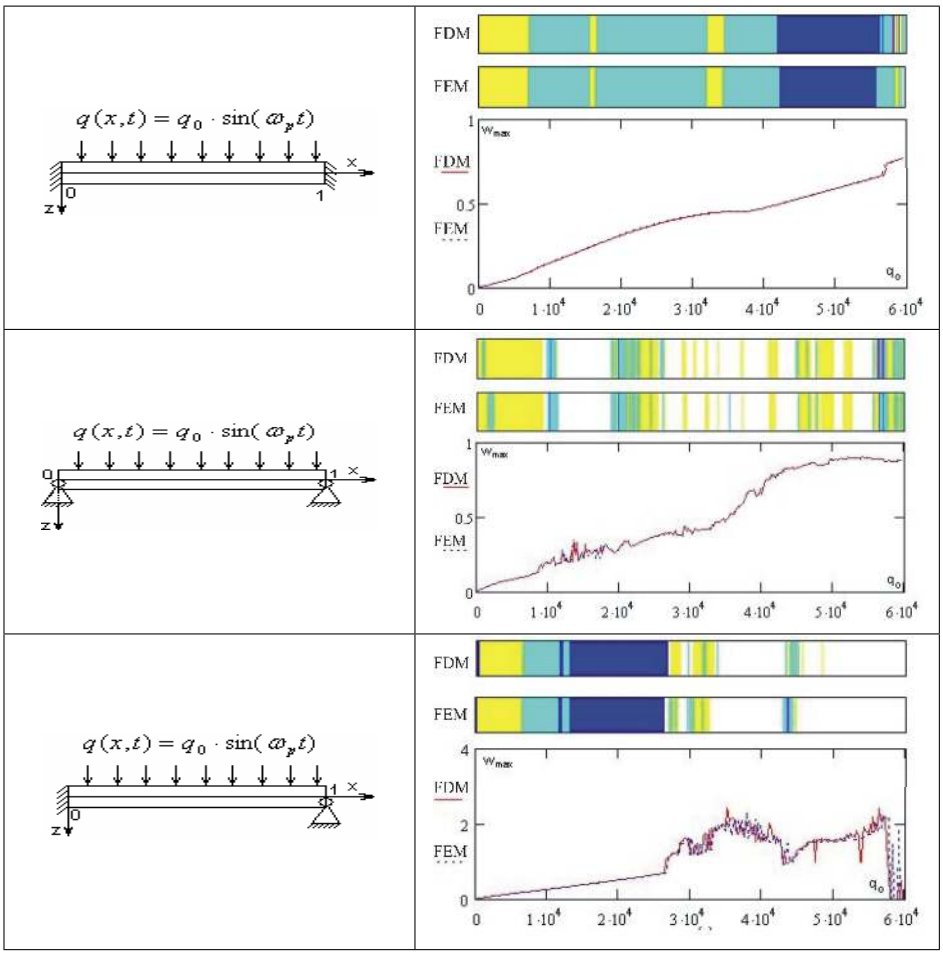

Table 2.5: Vibration scales, beam schemes and W_{max} obtained by FDM and FEM

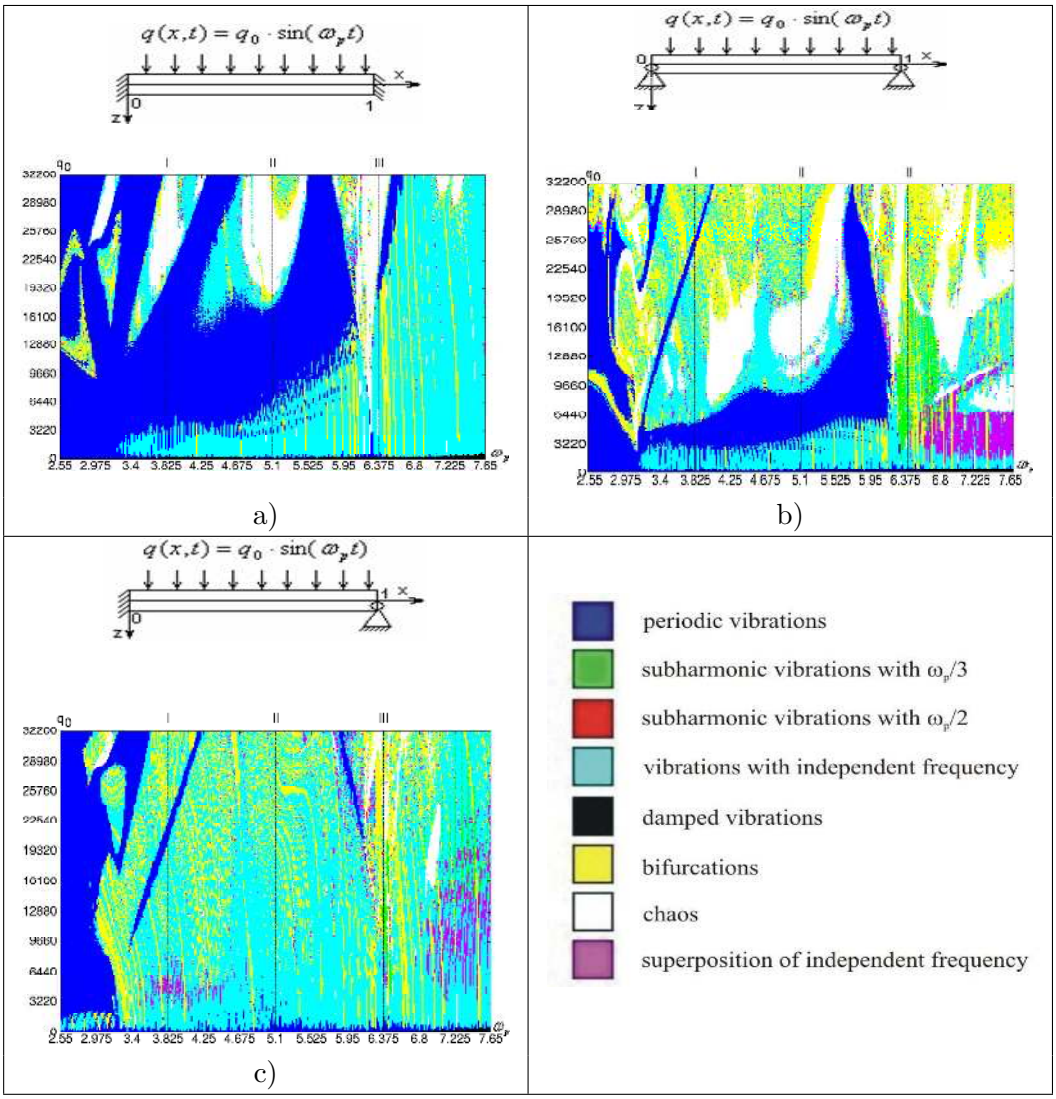

Table 2.6: Beam models and vibration type charts

Note that in the case of boundary conditions (4) - (a) and (6) - chart (c), the region of class "A" is the largest one. Besides, in chart (c) drops of bifurcation zones appear. Namely, small changes of the parameters $\{q_0, \omega_p\}$ cause a change of vibration regime, which is not required. Zones of class "B" are denoted in charts (a) and (b) and begin with the loading amplitude $q_0 \approx 19000$ - chart (a) and $q_0 \approx 7500$ - chart (b). It should be emphasized that zones of class "B" for a "simple support" are wider in comparison to "stiff clamping". Chart (c) essentially differs from charts (a) and (b), since it suffers from the lack of chaotic zones.

One of the important questions which appear in the investigation of chaotic beam vibrations is the analysis of a scenario transition from regular to chaotic motion. Next, we study the scenario for fixed $\omega_p = 9.2$ (Table 2.7) by FDM.

q_0	Sw	wt	$w(\dot{w})$
100	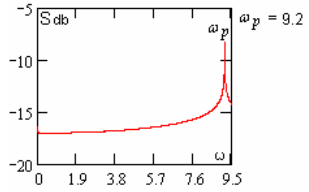	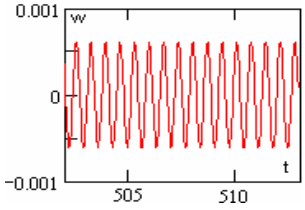	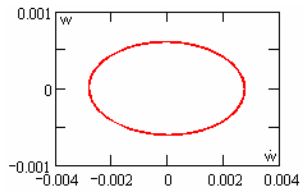
8740	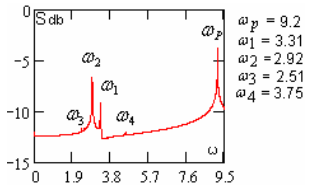	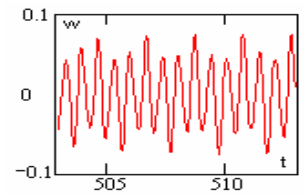	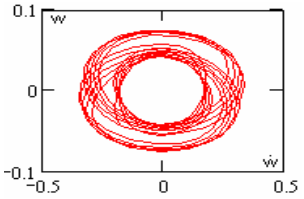
10500	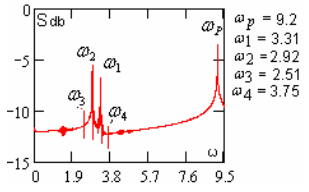	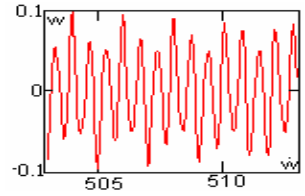	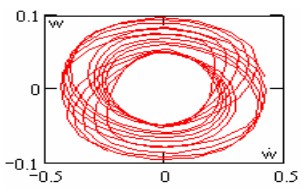
60000	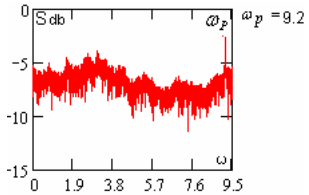	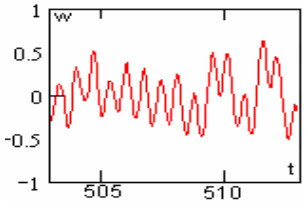	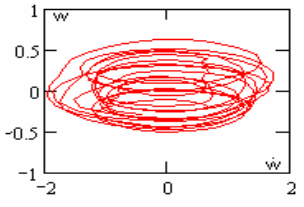

Table 2.7: Frequency spectra, time histories and phase portraits for different q_0 (Ruelle-Takens-Newhouse scenario)

The following transition steps are remarkable.

1. $q_0 = 100$. Periodic vibrations with excitation frequency ω_p.

2. $q_0 = 560$. Emergence of the first and second independent frequencies $\omega_1 = 3,31$, $\omega_2 = 2,92$.

3. $q_0 = 8740$. Occurrence of the third frequency $\omega_3 = 2,51$ and fourth frequency $\omega_4 = 3,75$. Simultaneously, the values of ω_1, ω_2 are changed and the following linear combination appears ω_1-ω_2=ω_2-ω_3.

4. $q_0 = 10500$. Noisy character of frequencies appears, and a chaotic component is observed. The combination of linear frequencies is as follows: ω_1-ω_2=ω_2-ω_3=ω_1-ω_4.

5. $q_0 = 60000$. Chaotic state of the system.

The so far reported scenario follows the so called Ruelle-Takens-Newhouse scenario presented in reference [3].

Below, the transition from regular to chaotic dynamics for $\omega_p = 6.2$ is illustrated. The following vibration steps are observed.

1. $q_0 = 50$. Periodic system vibrations with frequency $\omega_p = 6.2$. Then $\omega_1 = 0,07$ appears, whose value is successively decreased.

2. $q_0 = 9812.5$. Frequency ω_1 vanishes.

3. $q_0 = 9812.70887900199977594$. Sharp transition into chaos is observed.

4. $q_0 = 10300$. The system leaves the chaotic state and the associated frequencies are changed. Beside the excitation frequency, also two more appear, i.e. $\omega_2 = 1,57$ and $\omega_3 = 4,62$, and the difference between ω_P and ω_3 is ω_2. Pairs of frequencies around ω_2 and ω_3 appear. Their number increases up to a certain threshold, then the pairs of frequencies begin to vanish, and simultaneously the values of frequencies ω_2 and ω_3 are oscillating.

5. $q_0 = 16000$. For ω_2 the mentioned pairs of frequencies are $\omega_4 = 0,61$ and $\omega_7 = 2,79$; $\omega_5 = 1,08$ and $\omega_6 = 2,32$, whereas for ω_3 the pairs of frequencies are $\omega_8 = 3,40$ and $\omega_{11} = 5,5837$; $\omega_9 = 3,8779$ and $\omega_{10} = 5,1143$.

   A further increase of the load amplitude generates an increase of the number of the mentioned pairs of frequencies.

6. $q_0 = 23000$. The frequency ω_{12}=$\frac{\omega_P}{2}$ = is isolated, and the pair frequencies appear in its vicinity; also period doubling bifurcations are observed (region I).

7. $q_0 = 23500$. In the frequencies spectrum a chaotic component appears, and then the system transits into the chaotic regime.

The illustrated and studied scenarios are reported for the same problem, however for different excitation frequencies. Note that for different values of ω_p, the system is transited into chaotic state using different scenarios.

q_0	Sw	wt	$w(\dot{w})$
50	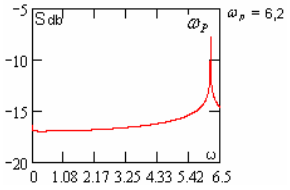	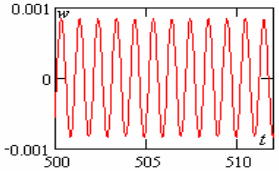	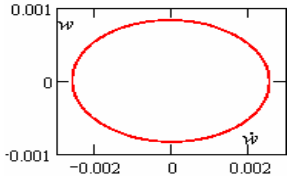
9812,5	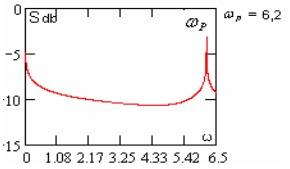	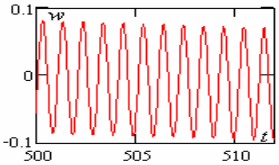	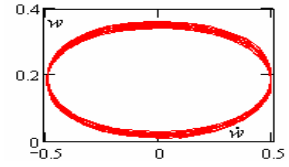
9812,7088...	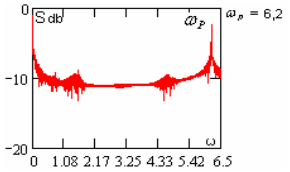	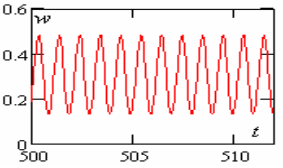	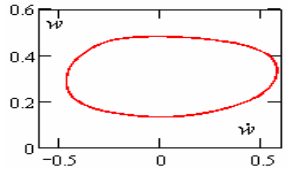
10300	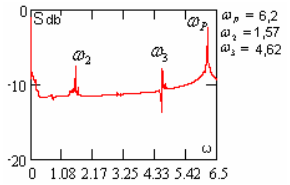	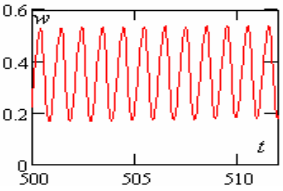	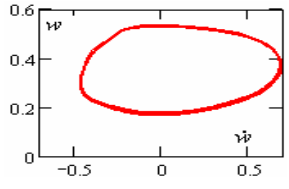
16000	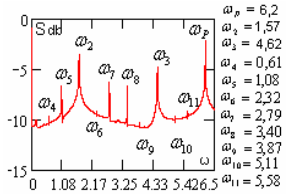	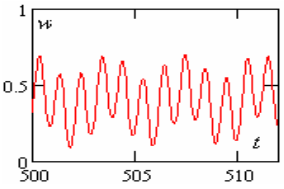	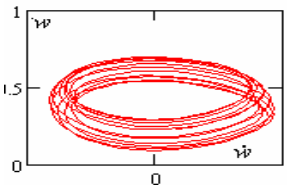
23000	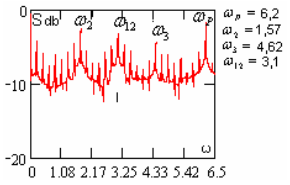	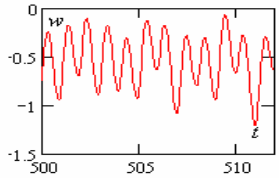	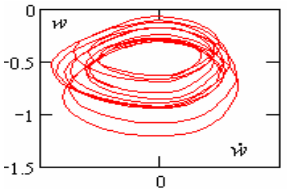
23500	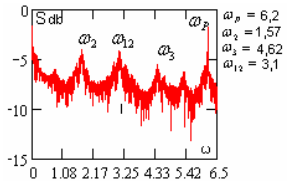	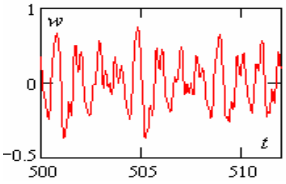	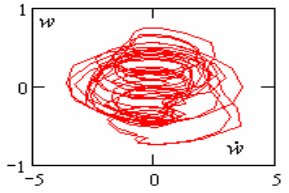

Table 2.8: Frequency spectra, time histories and phase portraits for different q_0

3.6 Chaotic beam vibrations excited by an impact

In this section, we study the case when a free beam edge is subjected to an impact of a rigid body with mass M_r and given velocity V. The problem described so far, beside a theoretical importance has also practical aspects. Namely, vibration processes are often generated by an impact which occurs during the contact of a spacecraft and orbital station, a rail-coach with a train, and so on. After impact the impacting body sticks with the beam and further the "beam + body" system is studied (Figure 2.2).

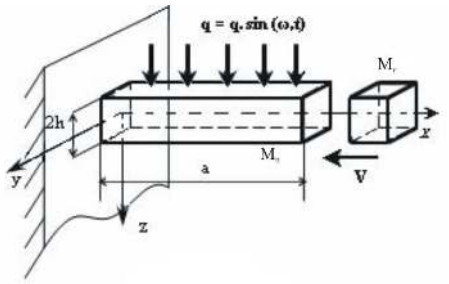

Figure 2.2: Impact between two bodies

In the impact time instant, owing to the 2nd Newton law, the following force $N_x \cdot (2h) = M_r \cdot \frac{\partial^2 u}{\partial t^2}$ appears on the free beam edge, where $2h$ denotes the beam height, M_r is the impacting body mass, $u(x,t)$ describes displacements along OX axis, and N_x is the longitudinal force. The associated non-dimensional governing equation form is as follows: $\frac{\partial^2 u}{\partial t^2} = \frac{1}{\chi} N_x$, where $\chi = \frac{M_r}{M_b}$, and M_b are the beam mass.

Finally, the mathematical model of beam vibrations during impact consists of the following parts:

i. Differential equations

$$\begin{cases} \frac{\partial^2 u}{\partial x^2} + L_3(w,w) - \frac{\partial^2 u}{\partial t^2} - \varepsilon_2 \frac{\partial u}{\partial t} = 0, \\ \frac{1}{\lambda^2}\left\{ L_2(w,w) + L_1(u,w) - \frac{1}{12}\frac{\partial^4 w}{\partial x^4} \right\} - \frac{\partial^2 w}{\partial t^2} - \varepsilon_1 \frac{\partial w}{\partial t} + q = 0; \end{cases} \tag{2.17}$$

ii. Boundary conditions

$$w(0) = u(0) = M_x = 0; \frac{1}{\chi} N_x = \frac{\partial^2 u}{\partial t^2}; \tag{2.18}$$

iii. Initial conditions

$$w(x)|_{t=0} = u(x)|_{t=0} = 0;$$

	$\lambda = 30$	$\lambda = 40$	$\lambda = 50$	$\lambda = 60$
$V = 0.05$	$t_{cr} = 1428,6$	$t_{cr} = 3891,8$	$t_{cr} = 1659,56$	$t_{cr} = 378,03$
$V = 0.01$	$t_{cr} = 611,91$	$t_{cr} = 486,72$	$t_{cr} = 322,72$	$t_{cr} = 175,5$

Table 2.9: Dependences of t_{cr} on λ and V

$$\frac{\partial w\left(x,t\right)}{\partial t}\left|_{t=0}=0;\frac{\partial u\left(x,t\right)}{\partial t}\right|_{t=0}=0 for x\neq 0,$$

$$\frac{\partial u\left(x,t\right)}{\partial t}_{t=0}=V for x=0. \tag{2.19}$$

We study nonlinear beam vibrations for: $X = 0.01$, $\omega_p = 5.1$; and when the beam is subjected to the action of constant transversal load $q = 10^{-7}$, free beam face is exposed to the impact of the rigid body side moving with velocity $V = 0.05, 0.1$, and the following damping coefficients are taken $\varepsilon_1 = 10^{-3}, \varepsilon_2 = 0$. Geometric beam parameters are: $\lambda = 30, 40, 50, 40$. Note that the impact generates longitudinal waves and their reflection. So, we introduce time t_{cr}, when a multiple interaction of the longitudinal waves occurs with appearing transversal waves.

Further, we study the dependence of t_{cr} on geometric beam parameters and on the impacting body velocity in the impact time instant.

As it is seen in Table 2.9, the value of t_{cr} is high in the case of relatively thick beams $\lambda = 30, 40$ and depends on the body velocity. We discuss the computational results of signals $w\left(t\right)$ and frequency power spectra $S_{db}\left(\omega\right)$ for each of the considered cases.

Analysis of the reported data shows that for small impacting body velocity periodic and damped vibrations appear. Increase of velocity yields a transition from longitudinal to transversal beam vibrations, what is well visible on the beam signal shapes. For $\lambda = 40$ and $V = 0.05$ the vibration process is slightly modified, and for remaining λ the beam vibrations are chaotic (in the reported case they are periodic).

3.7 Investigation of three-layered beam vibrations

The three-layered Bernoulli-Euler beam is investigated for the following parameters: $\lambda = 50$, $\varepsilon_1 = 0.1$, $\varepsilon_2 = 0.1$, $\omega_p = 5.1$. The amplitude of exciting load is changed in the interval $q_0 \in [0; 7500]$. The material of external layers is glass-plastic ($E_1 = 18.7GPa$, $\rho_1 = 1.8 \cdot 10^3 kg/m^3$), whereas internal layer is made from aluminum ($E_0 = 73GPa$, $\rho_0 = 2.681 \cdot 10^3 kg/m^3$).

A mathematical model is built using the Bernoulli-Euler hypothesis for the whole package of layers and taking into account non-linear relation between deformations and displacements in the form proposed by Kármán [13]. The following modified modules of elasticity and density are introduced:

$$E = \left(2h\right)^{-1} \cdot \left(E_0 h_0 + 2E_1 h_1\right), \rho = \left(2h\right)^{-1} \cdot \left(\rho_0 h_0 + 2\rho_1 h_1\right). \tag{2.20}$$

V		$\lambda = 30$	$\lambda = 40$	$\lambda = 50$	$\lambda = 60$
0.05	Signal	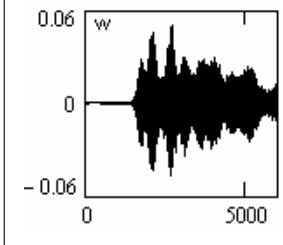	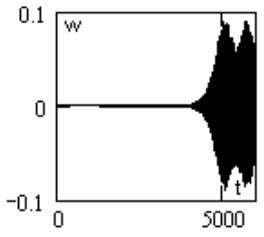	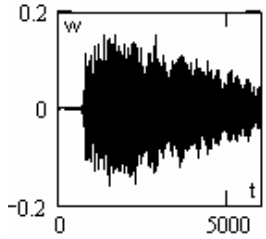	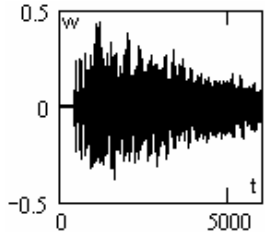
	Spectrum	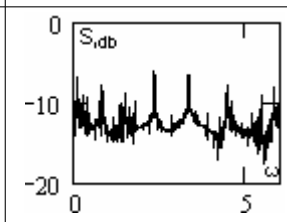	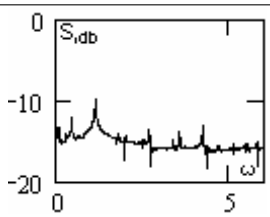	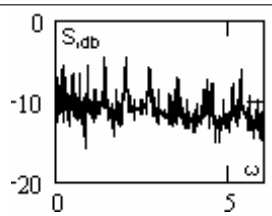	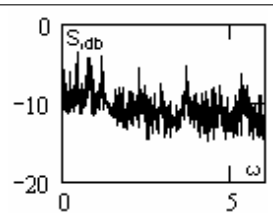
0.01	Signal	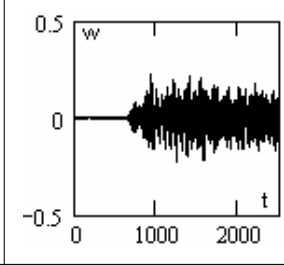	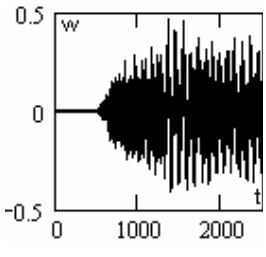	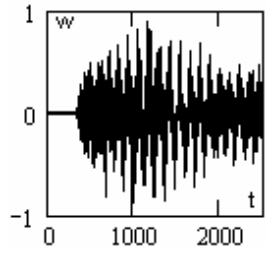	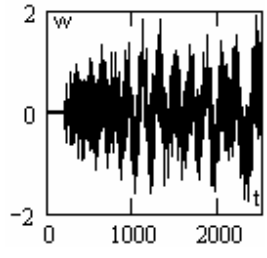
	Spectrum	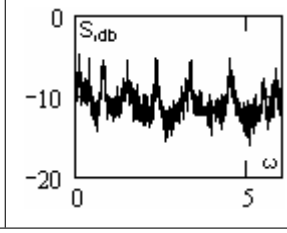	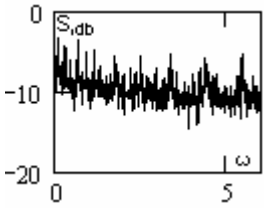	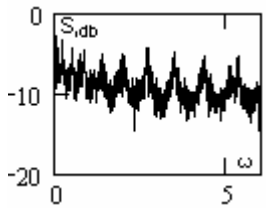	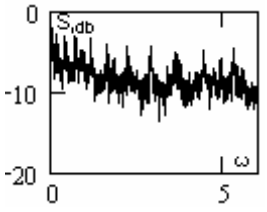

Table 2.10: Beam signals and frequencies for different λ and V

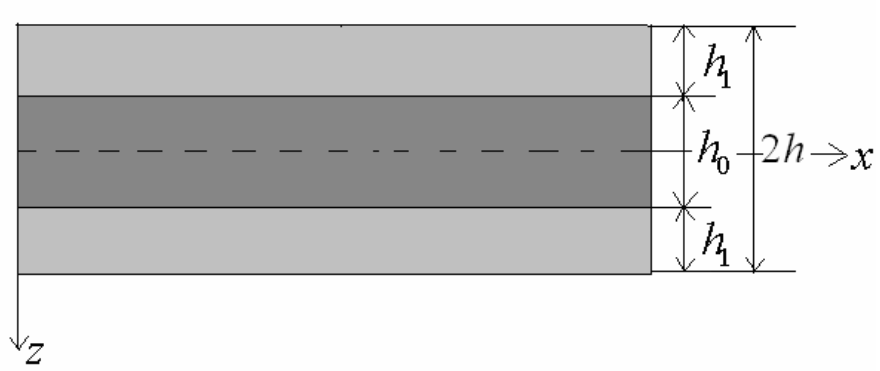

Figure 2.3: Three-layered beam

The model consists of differential equations (2.2), boundary conditions (2.6) and initial conditions (2.7).

Table 2.11 gives the functions of maximum deflection vs. amplitude of excitation, as well as vibration type scales. Results are given for different thicknesses of external layer h_1

$h_1 = h/5$	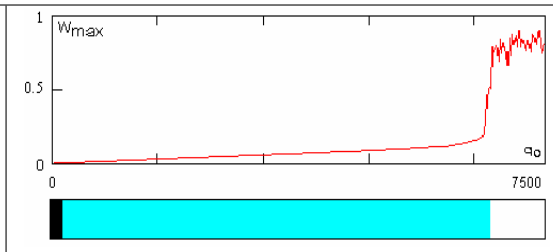	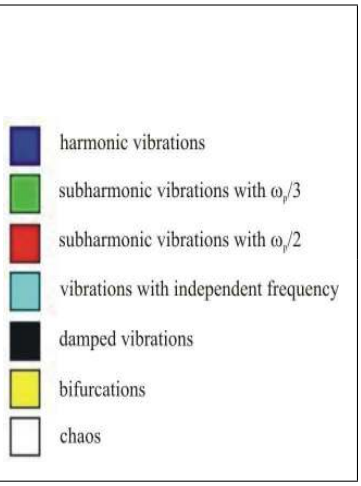
$h_1 = h/4$	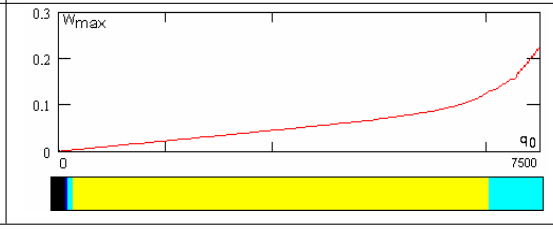	

Table 2.11: Functions W_{max} and vibration scales for different h_1

As Table 2.11 shows, the thickness of external layers has an essential influence on the vibrations of the three-layered symmetric beam. For instance, for external layer thickness $h_1 = h_2 = h/5$, and for loading amplitude $q_0 \in [500; 7000]$ vibrations take place with an independent frequency, whereas for $q_0 > 7000$ chaotic vibrations appear.

An increase of the external layer by 20% provokes an essential change in the development of the vibration scenario. For the load amplitudes $q_0 \in [700; 7000]$, the beam undergoes bifurcation type vibrations, whereas for the loading amplitude larger than 7000 periodic vibrations with an

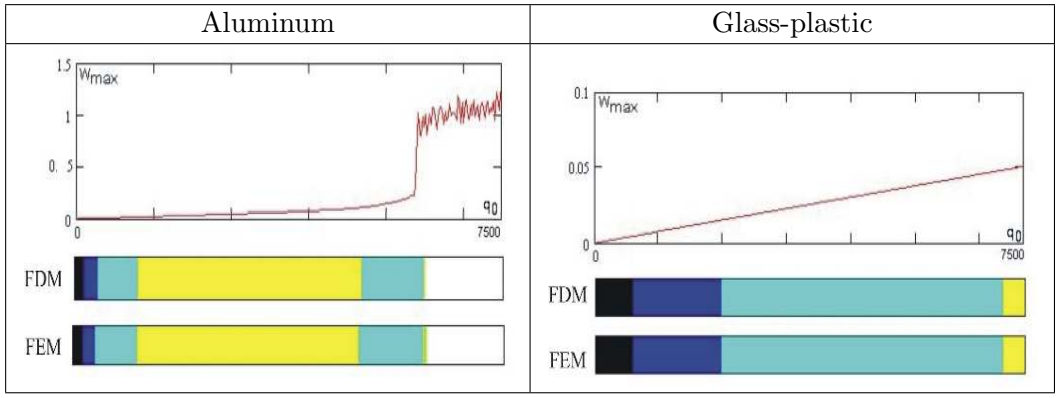

Table 2.12: Vibration scales and $w_{max}(q_0)$ obtained by FDM and FEM

independent frequency appear.

A transition from vibrations with independent frequency to chaotic vibrations for the external layer thickness of $h_1 = h/5$ is characterized by a jump of deflection in the function $\{w_{max}; q_0\}$. This shows that the so called stiff stability beam loss occurred, which may cause harmful effects. In this case in the function $\{w_{max}; q_0\}$ for external layer thickness $h_1 = h/4$, and during transition from the bifurcation to periodic regime a sudden change of deflection is not observed, and therefore stability loss does not appear.

Table 2.12 gives results for one-layered beams made from aluminum and glass-plastic. Computations are carried out for the same earlier used damping coefficients and excitation frequency.

The results are obtained due to the application of two mentioned computational methods (FDM and FEM). Although results presented on the graphs $\{w_{max}; q_0\}$ coincide in full, vibration scales exhibit slight differences only in the case of aluminum.

As it has been seen in Table 2.12, a one-layered beam made from glass-plastic does not vibrate chaotically within the whole interval of the applied loading. Vibration scales indicate that the vibrations with excitation frequency dominate. Beams made from aluminum exhibit chaotic dynamics for $q_0 \geq 6000$. Contrary to the beam made from glass-plastic, bifurcation vibrations dominate in this case. Similarly to results reported in Table 2.11, a transition to chaotic vibrations corresponds to a sharp change of beam deflection (aluminum), i.e. a stiff stability loss appears.

Comparison of the results presented in Tables 2.11, 2.12 shows that for external layer thickness $h_1 = h/5$ vibration type of the three-layered beam for $q_0 < 6000$ corresponds to vibrations of the beam made from glass-plastic, whereas for $q_0 \geq 6000$ beam vibrations are similar to those of the aluminum beam for the same loading amplitude excitation. In the case of external layer thickness $h_1 = h/4$ the behavior is completely inversed. It means that a slight change of layer thickness may qualitatively change the vibration behavior.

Therefore, one may control beam vibrations by changing the external layer thickness, i.e. stiffness beam properties. In other words, one may choose geometric parameters of the layers via numerical computations in such a way as to avoid harmful beam vibration regimes.

In order to study the second way of beam vibration control, we report charts of the vibration type vs. control parameters $\{q_0, \omega_p\}$ obtained through FDM (Table 2.13) for the beam package (where external layer thickness $h_1 = h/5$ - a), as well as for homogeneous material ($E = 2 \cdot 10^5$ MPa) - b). The vibration charts are constructed with the resolution 300×300, and the applied notation is the same as in Table 2.11.

In chart (a) large zones of damped vibrations dominate and the system (in general) vibrates with one independent frequency. Chaotic and bifurcation-type vibrations occupy very narrow zones. Observe that there are no regular vibration zones. For chart (b) the compression of chaotic zones is evident. Zones of damped vibrations are essentially smaller in comparison to those in chart (a), and they are distributed more uniquely. For low band frequencies and for loading amplitude up to 3000, zones of periodic vibrations appear. For high band frequencies, the image of vibrations is practically homogeneous and vibrations with independent frequency dominate.

In the case of multi-layered beams, their vibrations strongly depend on small frequency variations. Some frequencies are associated with chaotic dynamics within the whole interval of excitation amplitude. For the one-layered beam and for $\omega_p > 5.5$, the loading amplitude variation does not change the beam vibration type.

The charts of vibration types give a possibility to choose the required beam vibration regimes using two control parameters $\{q_0, \omega_p\}$, for which the beam exhibits either damped or harmonic vibrations with one independent frequency.

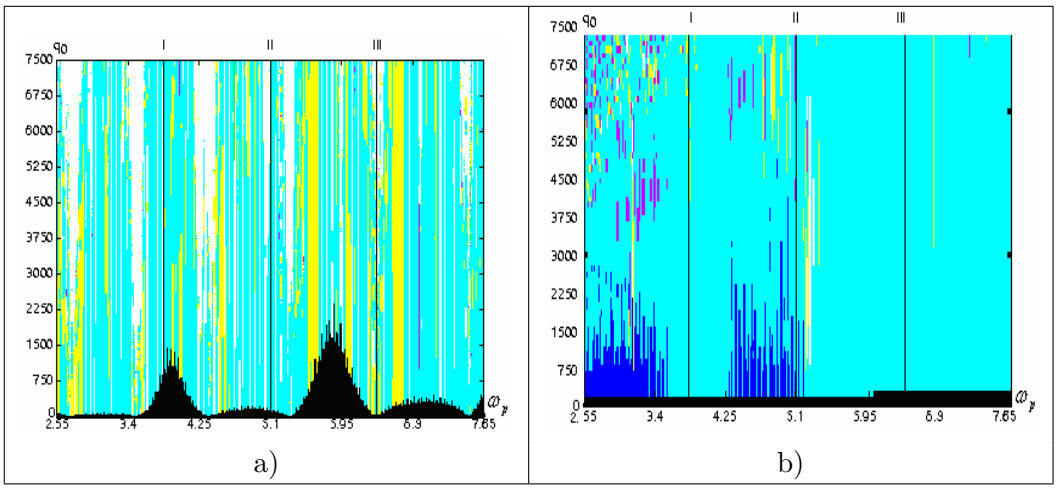

Table 2.13: Vibration charts of multiple (a) and single (b) beam layers

4 Numerical investigation of chaotic vibrations of flexible Timoshenko-type beams

4.1 Problem formulation

During construction of the mathematical model of the Timoshenko-type beam it is assumed that transversal cross sections remain flat after deformations, but they are not perpendicular to the middle beam axis [13]. In this model we take into account the angle between transversal cross sections and beam axis after deformation, which results in an increase of the number of functions being sought, keeping the unchanged order of ODEs.

The system of ODEs regarding displacements which govern the beam dynamics taking into account transversal shears effects (Timoshenko-type model) and energy dissipation in the non-dimensional form (non-dimensional parameters are defined by (2.1), and $\bar{\gamma} = \frac{\gamma a}{(2h)}$ - transversal shear), and for $\bar{\varepsilon}_3 = \varepsilon_3 \frac{a}{c}$ (damping coefficient associated with γ), takes the following form

$$\begin{cases} \frac{1}{3}\left(\frac{\partial^2 w}{\partial x^2} + \frac{\partial^2 \gamma_x}{\partial x^2}\right) + \frac{1}{\lambda^2}\left(L_1(w,u) + \frac{1}{2}L_2(w,w) + L_3(w,u) + L_2(w,w)\right) + \\ +2\frac{1}{\lambda^2}q - \frac{\partial^2 w}{\partial t^2} - \varepsilon_1 \frac{\partial w}{\partial t} = 0, \\ \frac{\partial^2 u}{\partial x^2} + L_4(w,w) - \frac{\partial^2 u}{\partial t^2} - \varepsilon_2 \frac{\partial u}{\partial t} = 0, \\ \frac{\partial^2 \gamma_x}{\partial x^2} - 8\lambda^2\left(\frac{\partial w}{\partial x} + \gamma_x\right) - \frac{\partial^2 \gamma_x}{\partial t^2} - \varepsilon_3 \frac{\partial \gamma_x}{\partial t} = 0; \end{cases} \tag{3.1}$$

where $L_1(w,u) = \frac{\partial^2 w}{\partial x^2}\frac{\partial u}{\partial x}$, $L_2(w,w) = \frac{\partial^2 w}{\partial x^2}\left(\frac{\partial w}{\partial x}\right)^2$, $L_3(w,u) = \frac{\partial w}{\partial x}\frac{\partial^2 u}{\partial x^2}$, $L_4(w,w) = \frac{\partial w}{\partial x}\frac{\partial^2 w}{\partial x^2}$ and bars over non-dimensional parameters are already omitted.

The system of ODEs (3.1) is supplemented by one of the following boundary and initial conditions

i. "Clamping - clamping":

$$w(0,t) = w(a,t) = 0; u(0,t) = u(a,t) = 0;$$

$$\gamma_x(0,t) = \gamma_x(a,t) = 0; \frac{\partial w(0,t)}{\partial x} = \frac{\partial w(a,t)}{\partial x} = 0; \tag{3.2}$$

ii. "simple support - simple support"

$$w(0,t) = w(a,t) = 0; u(0,t) = u(a,t) = 0;$$

$$Q_x(0,t) = Q_x(a,t) = 0; \frac{\partial^2 w(0,t)}{\partial x^2} = \frac{\partial^2 w(a,t)}{\partial x^2} = 0; \tag{3.3}$$

iii. "clamping - simple support"

$$w(0,t) = w(a,t) = 0; u(0,t) = u(a,t) = 0;$$

$$\gamma_x(0,t) = Q_x(a,t) = 0; \frac{\partial w(0,t)}{\partial x} = \frac{\partial^2 w(a,t)}{\partial x^2} = 0; \tag{3.4}$$

iv. “clamping - free edge”

$$w(0,t) = u(0,t) = 0; \gamma(0,t) = \frac{\partial w(0,t)}{\partial x} = 0;$$
$$M_x(a,t) = N_x(a,t) = Q_x(a,t) = 0; \tag{3.5}$$

and the initial conditions are

$$w(x,t)_{|t=0} = u(x,t)_{|t=0} = \gamma(x,t)_{|t=0} = 0,$$
$$\frac{\partial w(x,t)}{\partial t}_{|t=0} = \frac{\partial u(x,t)}{\partial t}_{|t=0} = \frac{\partial \gamma_x(x,t)}{\partial t}_{|t=0} = 0. \tag{3.6}$$

4.2 Solution of PDEs via FDM and FEM

The studied infinite system is solved by FDM with the approximation of $O\left(c^2\right)$ and is reduced to a system of finite ODEs. In each mesh node the following ODEs are obtained

$$L_{1,c}(w,u,\gamma) = \varepsilon_1 \dot{w}_i + \ddot{w}_i,$$
$$L_{2,c}(w,u) = \varepsilon_2 \dot{u}_i + \ddot{u}_i,$$
$$L_{3,c}(w,\gamma) = \varepsilon_3 \dot{\gamma}_{x_i} + \ddot{\gamma}_{x_i}. \tag{3.7}$$

Boundary and initial conditions are also presented in the difference form which are analogous to equations (2.9) - (2.11) but with inclusion of γ_x.

Applying the Bubnov-Galerkin procedure, the following FDM equations are obtained

$$\begin{cases} M_1\left[\ddot{W}\right] + C_1\left[\dot{W}\right] + K_1[W] = F_1(q,U,\varphi), \\ M_2\left[\ddot{U}\right] + C_2\left[\dot{U}\right] + K_2[U] = F_2(W), \\ M_3[\ddot{\varphi}] + C_3[\dot{\varphi}] + K_3[\varphi] = F_3(W). \end{cases} \tag{3.8}$$

The system of equations (3.5) and (3.6) is solved via a standard procedure of the 4th order Runge-Kutta method.

4.3 Reliability of the obtained results

In order to check reliability of the obtained results for the Timoshenko-type model, solutions obtained via FDM and FEM are compared. Next, we study the problem for boundary conditions of clamping-clamping, simple support-simple support, clamping-simple support for the same parameters as in the Bernoulli-Euler beam investigations ($\varepsilon_3 = 0$).

Graphs of the dependencies of the maximum deflection vs. excitation amplitude are obtained via different computational methods. They fully coincide in the case of regular beam vibrations, whereas slight differences appear only for chaotic dynamics.

On the basis of results presented in Table 3.1, one may conclude that for the excitation amplitude corresponding to regular vibrations the values of w_{max} coincide fully for two applied computational approaches. In the case of chaotic dynamics small differences are visible. Vibration scales obtained by the two methods fully coincide. Transition to chaos appears using FDM later than in the case of FEM computation and the chaotic regime is smaller in the case of applied FDM approach.

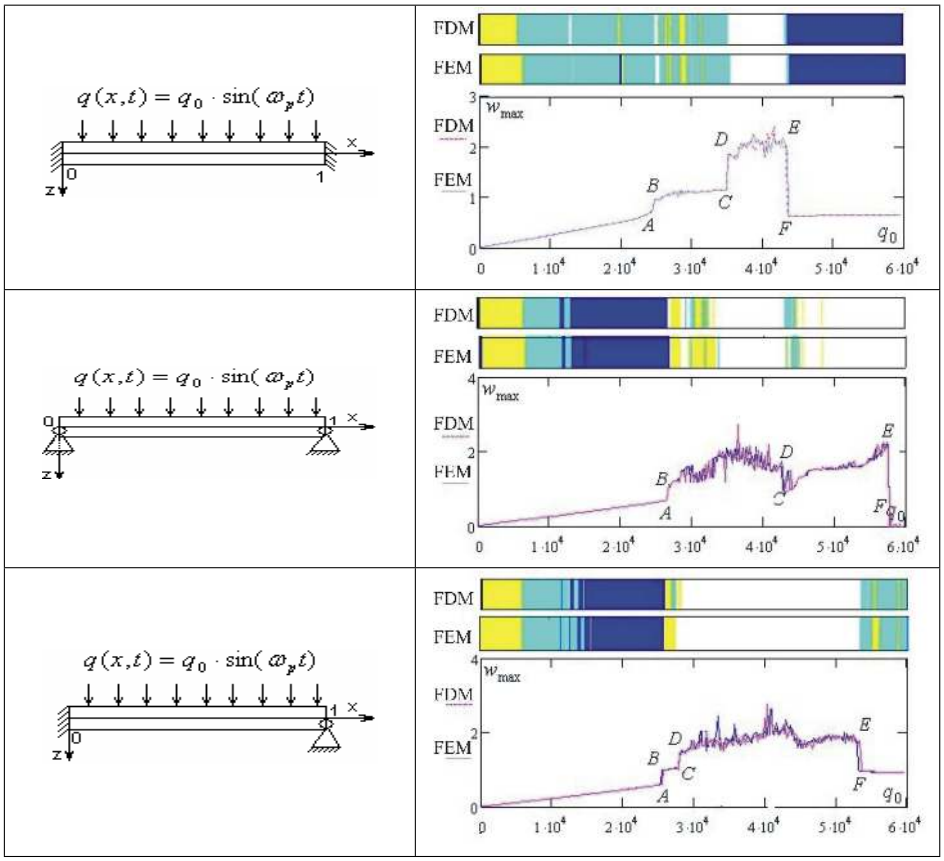

Table 3.1: Beam schemes, Vibration scales, beam schemes and $W_{max}(q_0)$ obtained by FDM and FEM

Observe that dynamical stability loss of the beam transversally excited by sign-changeable load occurs, which is characterized by a sharp change of the maximum deflection associated with a small change of the excitation amplitude. Dynamical stability loss occurs during the transition from point A to point B, and from point C to point D. These transitions are associated with the occurrence of chaotic zones. During the transition form point E to point F inversed transition occurs, i.e. from chaos to regular dynamics, which is also presented on a scale (in the last case the beam deflection values are decreased by about 1.5 times).

Charts showing dependence of vibrations character vs. control parameters (Table 3.2) for the Timoshenko-type beam are also presented for the used FDM (a) and FEM (b). Analysis of scales and charts included in Tables 3.1 and 3.2 supports the earlier conclusion on a significant influence of the transversal shear effects, keeping the same parameters of the used mathematical beam models. A comparison of charts for the Timoshenko and Euler-Bernoulli beams shows that for the same initial and boundary conditions and control parameters, the charts differ from each other significantly. For instance, chaotic (periodic) zones (Table 3.2 a) are wider (narrow) than those presented in Table 3.2b. A characteristic feature of the two mentioned charts is that vibrations with independent frequency dominate. This suggests a need of development of more exact mathematical models.

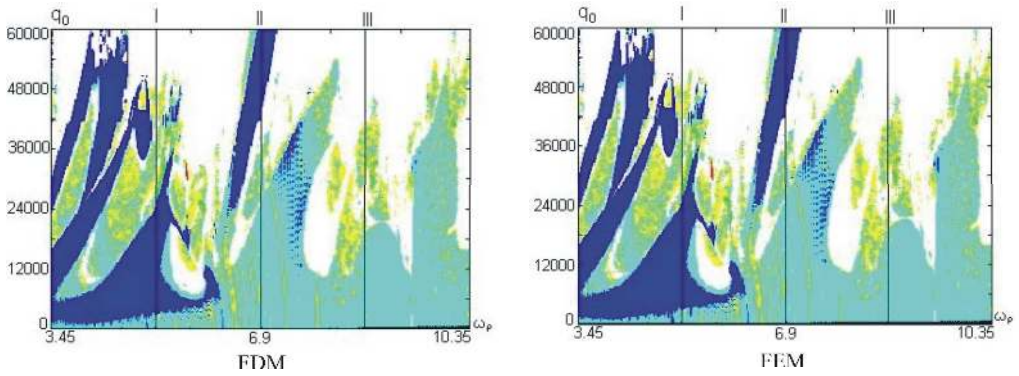

(a) (b)

Table 3.2: Beam vibration charts obtained by FDM (a) and FEM (b)

4.4 Chaos vs. boundary condition variations

Next, we consider the influence of boundary conditions on the Timoshenko-beam vibrations (Table 3.3). The amplitude of excitation load is $q_0 \in [0; 60000]$ and the excitation frequency $\omega_p \in [3.45; 10.35]$. The remaining parameters are the same as in the case of the Bernoulli-Euler beam investigation. The classification of vibration types A and B is introduced like in part II.

The zones regarding class "A" practically have the same area for the presented three charts, differing only because of vibration types. Vibration regimes of class "B" begin from the external loading amplitude $q_0 \approx 12000$. In the chart associated with non-symmetric boundary conditions for $\omega_p \approx [7.8; 9.1], [9.8; 10.35]$ chaotic zones appear already for $q_0 \approx 10$.

Let us discuss in more detail scenarios shifting the investigated system from regular to chaotic dynamics. We consider three scenarios regarding frequencies: $\omega_p = 8.05, 6.9, 5.75$. As it is exhibited by the chart, the system is transited into chaos during the change of excitation amplitude. Table 3.4 gives fundamental steps of the mentioned scenario for $\omega_p = 8.05$ (FDM).

The following fundamental steps of the system behavior are detected.

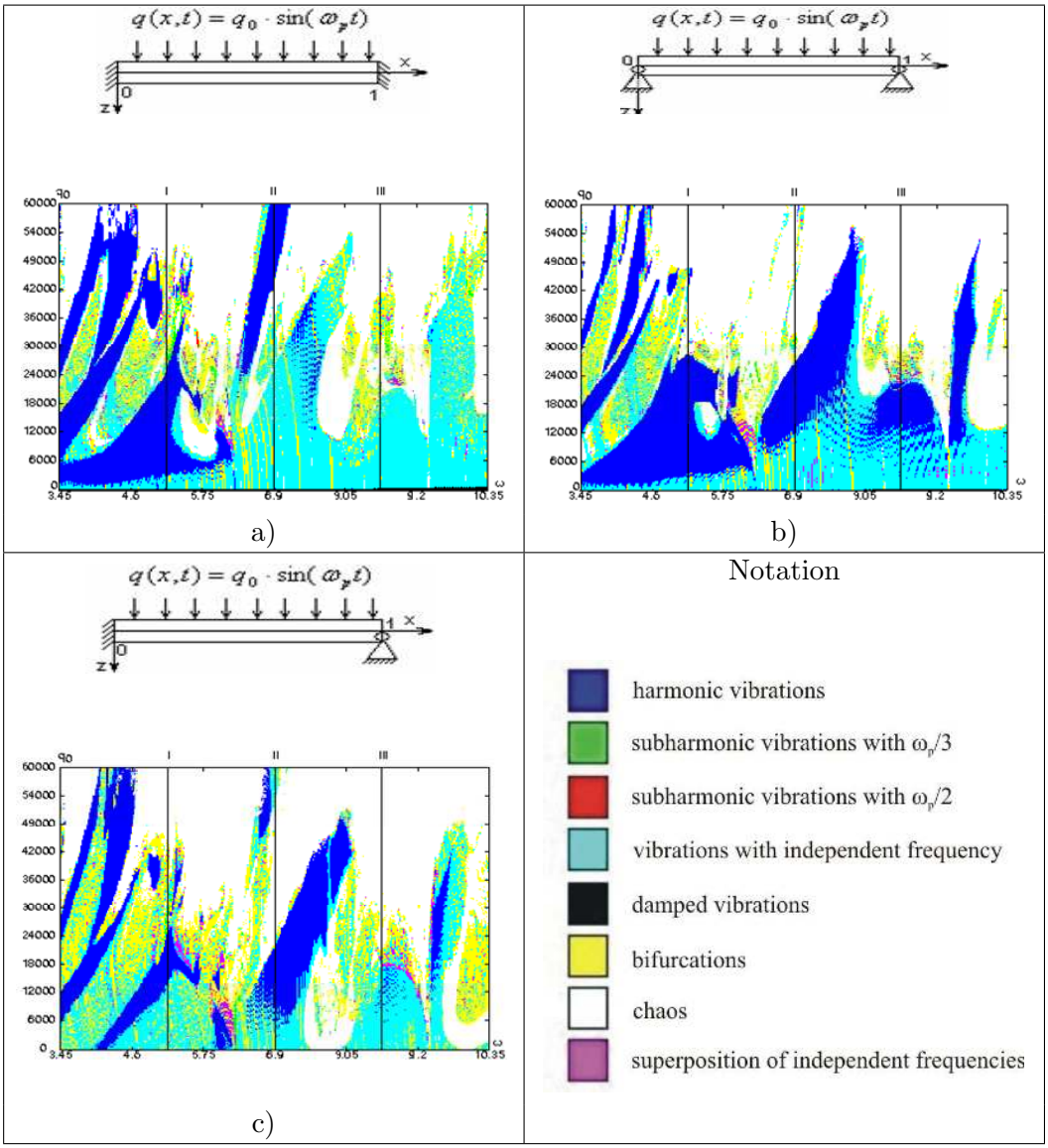

Table 3.3: Beam schemes and vibration charts

1. $q_0 = 1$. System vibrations are periodic, and only frequency excitation appears in the frequency spectrum.

   In the given interval three frequencies appear, which are linearly independent, i.e. $\omega_1 = 4.46$, $\omega_2 = 1.83$ and $\omega_3 = 4.9$.

2. $q_0 = 4600$. After occurrence of $\omega_4 = 0.92$, the following linear frequency relations appear: $\omega_2 - \omega_4 = 0.85$, and $\omega_3 - \omega_1 = 0.85$.

3. $q_0 = 11000$. Frequencies constitute three groups, where the linear dependence in each group follows: $\omega_1 - \omega_2 = \omega_2 - \omega_4 = 1.1$, $\omega_3 - \omega_1 = \omega_1 - \omega_6 = 1.1$, $\omega_p - \omega_5 = 1.1$.

4. $q_0 = 30000$. Frequency power spectrum exhibits first, second and third period doubling bifurcations denoted as I, II and III.

5. $q_0 = 40000$. The fourth period doubling bifurcation is detected, and the phase portrait consists of four rings.

6. $q_0 = 42500$. There are three bifurcations, and an inversed route from chaos to regular dynamics is realized.

7. $q_0 = 45000$. New frequencies appear, whose values differ from fundamental frequencies by the amount of 0.42, and the following relations hold $\omega_4 - \omega_1 = \omega_7 - \omega_4 = \omega_9 - \omega_7 = \omega_p - \omega_{10} = 1.86$.

The given scenario (for small values of the excitation amplitude) is characterized by three frequency vibrations. Then, a series of new frequencies, whose values depend linearly on the fundamental frequencies, appear and finally further frequency bifurcations yield a broad band frequency spectrum. The investigated system is transited through a chaotic zone, and then the number of bifurcations decreases.

Table 3.5 gives a scenario associated with excitation frequency $\omega_p = 6.9$ (FDM).

The following steps of beam dynamical behavior are detected.

1. $q_0 = 1000$. System vibrations are periodic, and the frequency spectrum consists of excitation and $\omega_1 = 0.627$ frequencies, and ω_1 does not depend linearly on ω_p.

2. $q_0 = 24000$. The following linearly dependent frequencies appear: $\omega_2 = \omega_p - 2\omega_1, \omega_3 = \omega_1 \cdot 3, \omega_4 = \omega_2 - 2\omega_1$. Then the frequency values are changed.

3. $q_0 = 24600$. The so far reported frequencies undergo three bifurcations denoted as I, II and III.

4. $q_0 = 25500$. The frequency spectrum consists of the following linearly dependent frequencies: $\omega_p - \omega_2 = \omega_2 - \omega_4 = \omega_4 - \omega_7 = 1.8$, $\omega_2 - \omega_6 = \omega_9 - \omega_4 = \omega_4 - \omega_3 = \omega_3 - \omega_{11} = = \omega_7 - \omega_1 = 0.53$

q_0	Sw	wt	$w(\dot{w})$
1	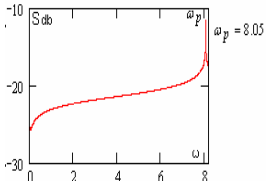	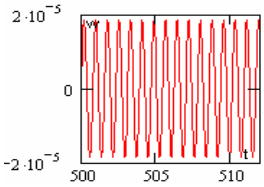	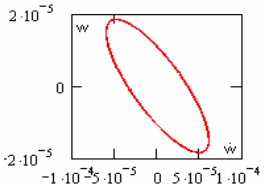
4600	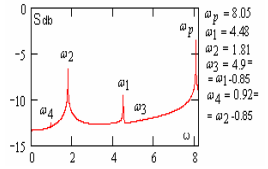	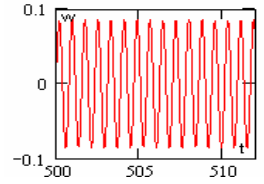	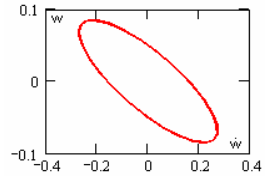
11000	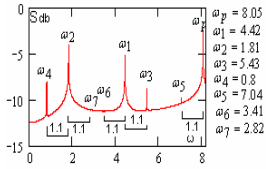	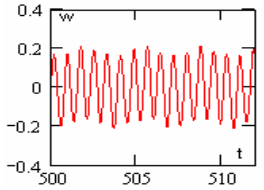	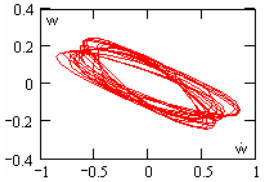
30000	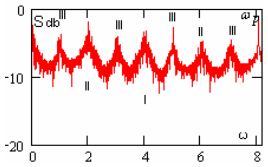	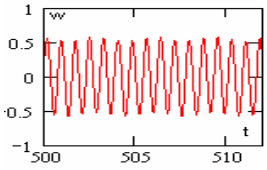	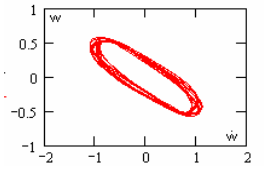
40000	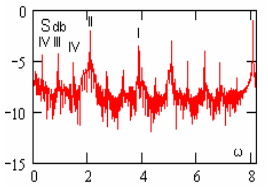	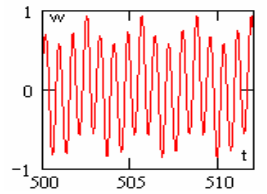	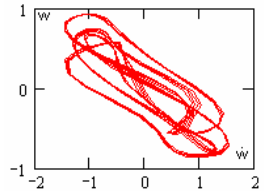
42500	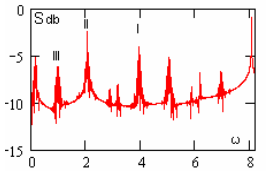	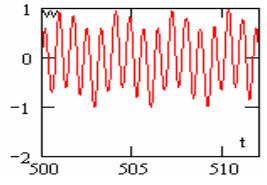	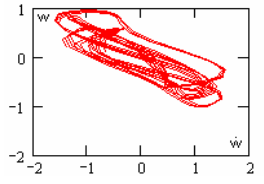
45000	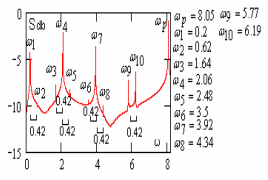	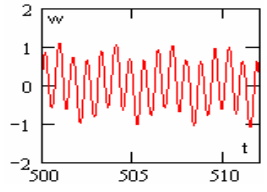	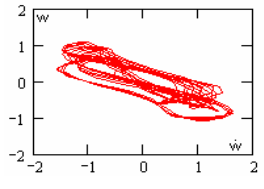

Table 3.4: Frequency spectra, time histories and phase portraits for different q_0 and $w_p = 8.05$

q_0	Sw	wt	$w(\dot{w})$
1000	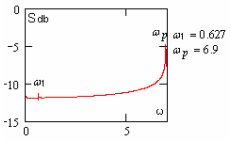	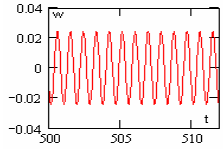	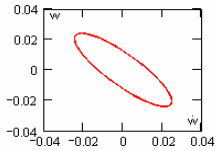
24000	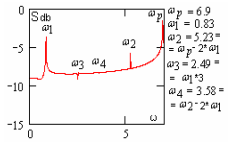	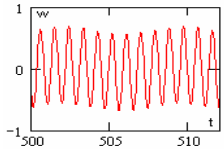	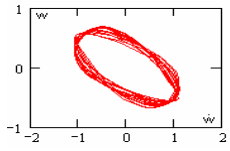
24600	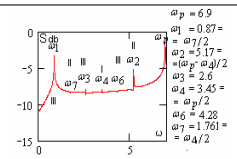	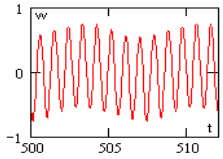	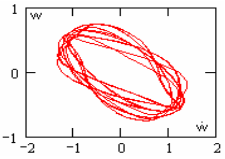
25500	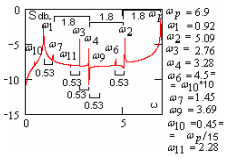	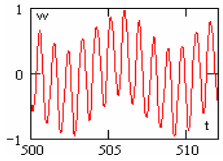	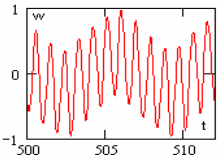
40000	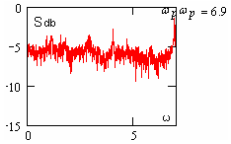	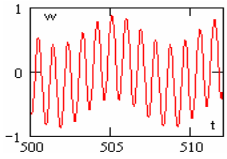	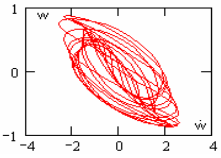
43000	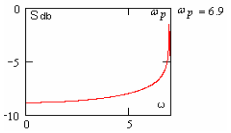	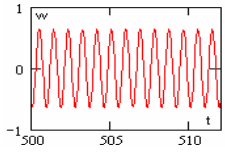	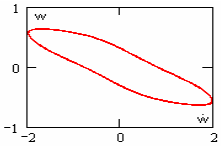

Table 3.5: Frequency spectra, time histories and phase portraits for different q_0 and $w_p = 8.05$

5. $q_0 = 40000$. The system exhibits chaos.

6. $q_0 = 43000$. Inversed transition from chaos to regular motion takes place.

In the considered case, the two-frequency system vibrations undergo three bifurcations associated with the occurrence of new linearly dependent frequencies and with the changes of the frequencies which appeared earlier. However, frequency values are changed further, and the system exhibits vibrations with four fundamental frequencies linearly dependent on ω_p. As a result of new linearly dependent frequencies, the system transits into chaos.

Table 3.6 presents the system behavior for $\omega_p = 5.75$ (FDM).

The following dynamical behavior of the system is tracked.

1. $q_0 = 1$. System vibrations are linear.

2. $q_0 = 6200$. Frequencies $\omega_1 = 0.46$ and $\omega_5 = 1.36$ are linearly independent, and the following relations hold: $\omega_p - \omega_7 = \omega_3 - \omega_2 = \omega_2 - \omega_6 = 1$.

3. $q_0 = 12000$. Frequency values differ from each other on 0.61.

4. $q_0 = 18000$. A large number of frequencies appear in the frequency spectrum and the fundamental frequencies depend on each other on the value of 0.169.

5. $q_0 = 19000$. The system returns to regular dynamics.

6. $q_0 = 20000$. First bifurcation associated with the frequency $\omega_2 = 2.87 = \omega_p/2$ appears.

7. $q_0 = 23750$. New frequencies linearly dependent on these described so far appear, i.e. $\omega_1 = 1.04, \omega_2 - \omega_3 = \omega_4 - \omega_2 = \omega_p - \omega_5 = \omega_1$.

8. $q_0 = 28000$. Frequency spectrum becomes broadband.

9. $q_0 = 40000$. The system is in a chaotic regime.

In the scenario three-frequency vibrations appear, which further are transited into linear combinations of all frequencies. The described scenario corresponds to the modified Ruelle-Takens-Newhouse scenario. Further, the system again exhibits periodic vibrations, and next the first bifurcation appears, and then period doubling bifurcation of ω_p and the first bifurcated frequency occur. Then, the system is transited into the chaotic state.

The reported results emphasize that in the control parameters $\{q_0, \omega_p\}$ plane there is no universal transition from regular to chaotic dynamics of the investigated system. There are subspaces of $\{q_0, \omega_p\}$, where the transition from regular to chaotic dynamics is realized in a different way.

q_0	Sw	wt	$w(\dot{w})$
1	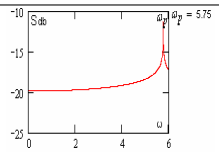	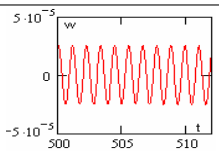	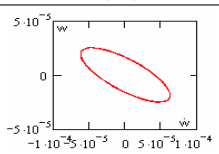
6200	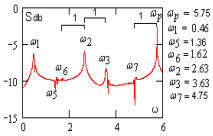	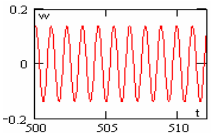	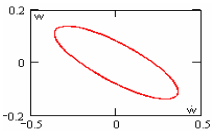
12000	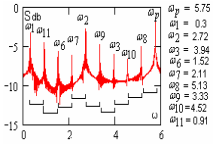	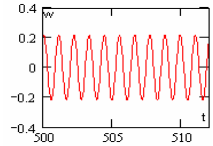	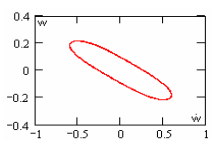
18000	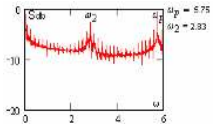	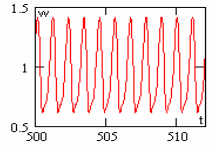	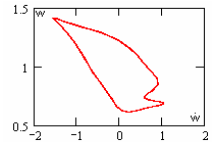
19000	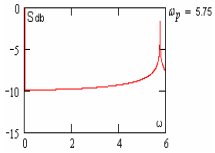	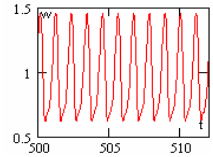	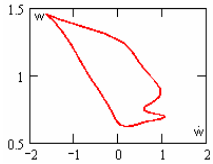
20000	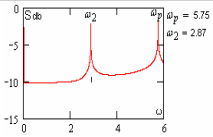	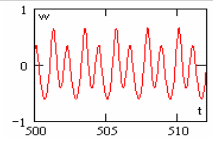	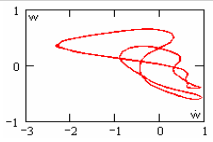
23750	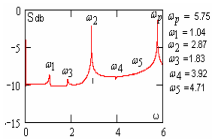	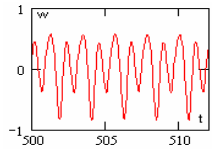	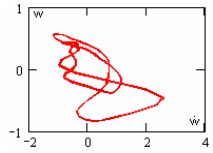
28000	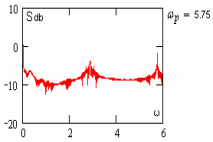	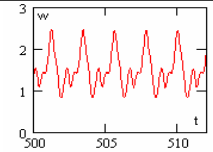	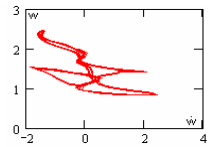
40000	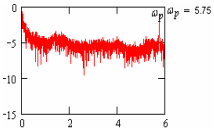	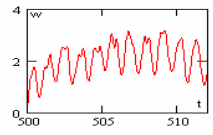	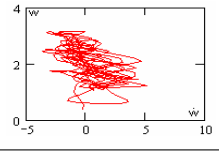

Table 3.6: Frequency spectra, time histories and phase portraits for $\omega_p = 5.75$

5 The Bernoulli-Euler model vs. Timoshenko model

The investigation of vibrations of non-linear constructions within different vibration regimes (periodic and chaotic) implies the need of improvement of mathematical models and computational techniques. Note that taking into account the transversal shear effect causes a qualitative change of the system dynamics. It is clearly illustrated by a comparison of the vibration type scales and charts constructed for different mathematical models (the Bernoulli-Euler and Timoshenko-type models) for the same parameters used during computation.

The reported vibration scales and dependencies $w_{max}\,(q_0)$ regarding the Bernoulli-Euler and Timoshenko-type are studied for all boundary conditions.

	The Bernoulli-Euler model	The Timoshenko-type model
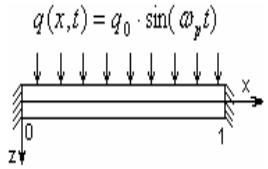	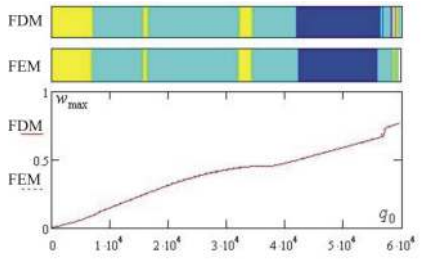	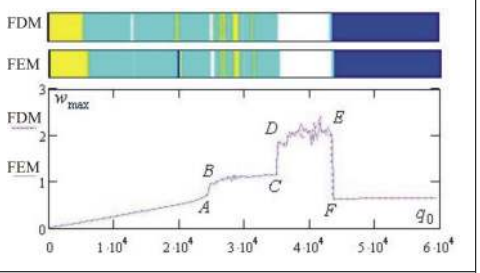
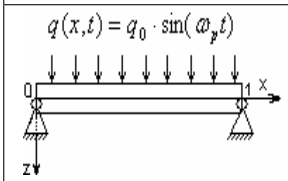	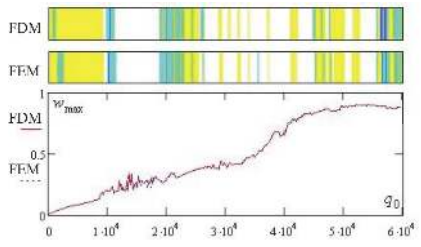	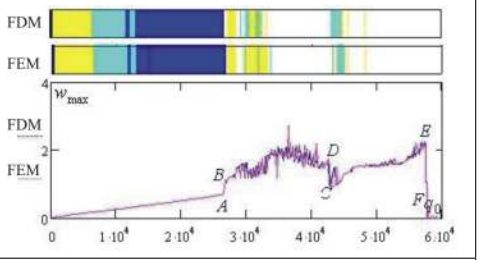
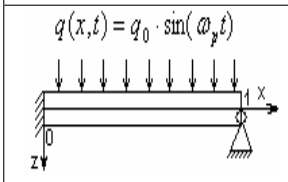	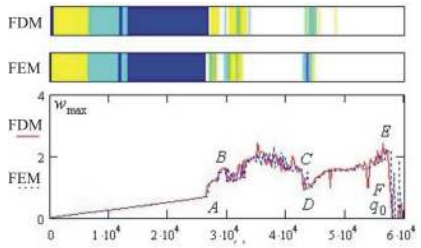	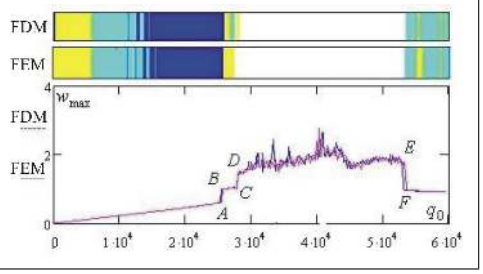

Table 4.1: Beam schemes, vibration scales and $w_{max}(q_0)$ for the Bernoulli- Euler and for the Timoshenko models obtained by FDM and FEM

Table 4.1 shows that the results obtained for the Bernoulli-Euler and Timoshenko-type mod-

els differ essentially regarding scales and functions $w_{max}(q_0)$. For hybrid types of boundary conditions the results converge in particular for $q_0 \leq 2.7 \cdot 10^4$. Observe that for symmetric boundary conditions for the Timoshenko-type model a stiff stability loss appears, when the system is driven by transversal sign-changeable load. However, for the Bernoulli-Euler model the transition into chaos is associated with a rather smooth change of the maximum beam deflection.

Next, we study vibration type charts, the control parameter planes for the Bernoulli-Euler model and the Timoshenko-type model for three different boundary conditions (see Table 4.2).

Since the free beam frequencies, as well as beam vibration amplitudes do not coincide for both studied models for the maximum deflection $5\,(2h)$, the charts reported in Table 4.2 are constructed for different values of control parameters (for the Bernoulli-Euler beam $\omega_p \in (2.55, 7.65)$, $q_0 \in (0, 32200)$, and for the Timoshenko-type beam $\omega_p \in (3.45, 10.35)$, $q_0 \in (0, 60000)$). Vibrations of the investigated system in the case of hybrid boundary conditions regarding the Bernoulli-Euler and Timoshenko-type models are similar to the case of symmetric boundary conditions but for different frequency intervals. The mentioned similarity has a remarkable mirror type character. Namely, for the Bernoulli-Euler model the chart coincides with the chart regarding simply supported beam ends, whereas for high frequencies –for clamped ends. The inversed behavior to that described so far takes place for non-symmetric boundary conditions of the Timoshenko-type model.

One more important question is that of beam modeling influence on the system behavior. We compare charts constructed for the same numerical values of control parameters for the case of the Bernoulli-Euler model and for the case of the Timoshenko-type model for the boundary conditions associated with stiff clamping (see Table 4.3).

Table 4.3 shows vibration type charts for the same parameters and for clamping-clamping beam boundary conditions.

Observe that zones of class B for the Timoshenko-type model are wider and begin with the amplitude $q_0 \approx 6000$ for the Timoshenko type model, whereas they begin with $q_0 \approx 12000$ for the Bernoulli-Euler model. However, zones of class A for the Timoshenko-type model are smaller in comparison to the Bernoulli-Euler model. Note that for $q_0 \in [0; 5000]$ beam deflection values are small and essentially the system behaves in a linear manner. The character of vibrations estimated by the two models practically coincides, which indicates their validation and reliability. Loading over $3 \cdot 10^4$, which essentially influences nonlinear terms in equations (2.2), (3.1), results in the occurrence of qualitative differences between results obtained via two mentioned beam models.

Furthermore, the introduction of transversal shear effects and rotation inertia (the Timoshenko model) essentially influences the character of beam vibrations. Additionally, the following observations result from the study of two charts regarding the applied beam models:

i. chaotic vibrations for the Timoshenko-type model are wider regarding either amplitude or frequency;

ii. zones of harmonic vibrations and zones of independent frequency vibrations are smaller in

	The Bernoulli-Euler model	The Timoshenko-type model
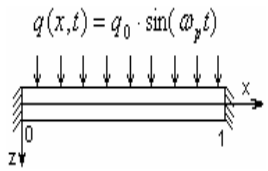	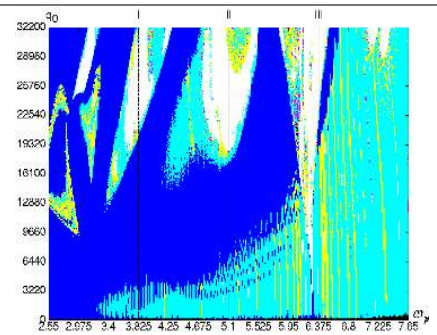	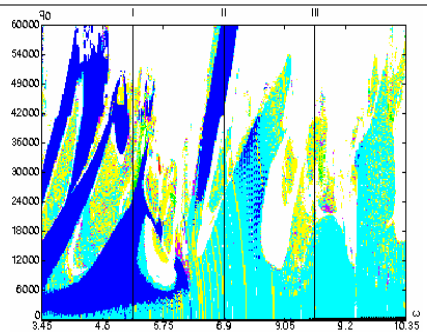
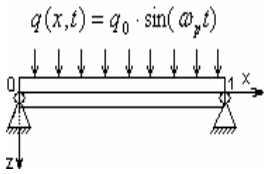	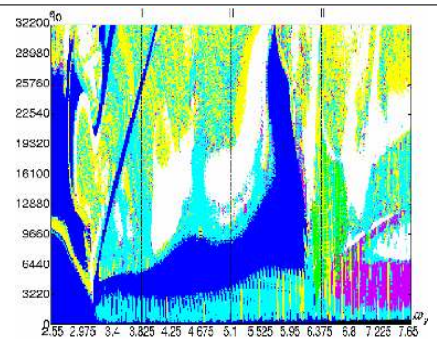	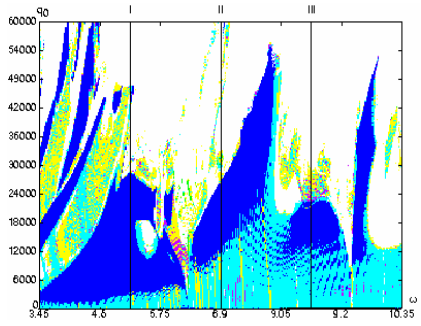
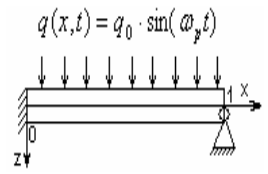	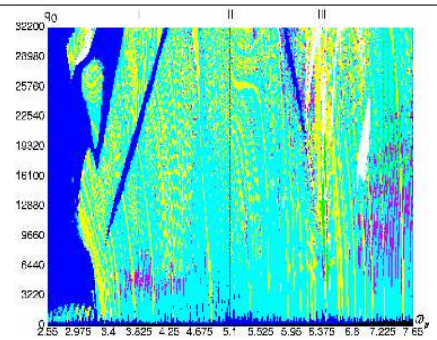	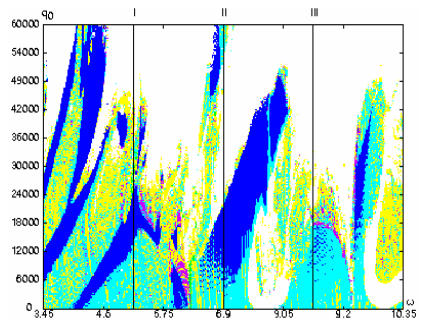

Table 4.2: Beam schemes and vibration charts for two models and three boundary conditions

	The Bernoulli-Euler model	The Timoshenko-type model
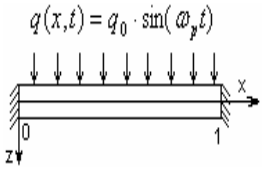	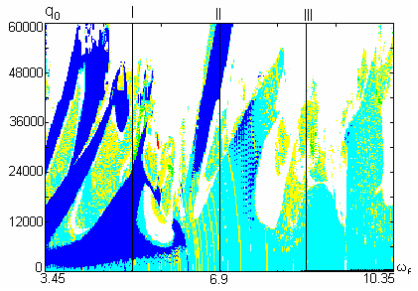	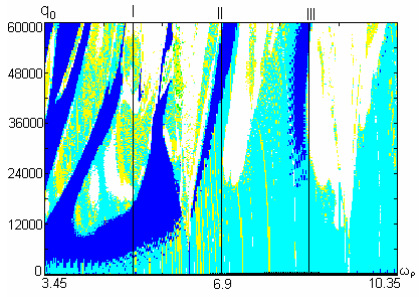

Table 4.3: Vibration charts for two models and stiff clamping

the case of Timoshenko-type model;

iii. the character of vibrations of two models coincides for low frequencies, but for higher frequencies the differences increase.

6 General conclusions

1. A general theory of nonlinear vibrations of flexible Bernoulli-Euler and Timoshenko-type beams is developed.

2. The equivalence of reduction of infinite input problem to finite dimensional one regarding a spatial coordinate by FDM with approximation of $O\left(c^2\right)$ and FEM in the form of the Bubnov-Galerkin is discussed and illustrated.

3. Note that for a computer with a Celeron 1700 processor, computational time of the FDM is by 1.5-1.7 times shorter than for the FEM method.

4. Scenarios of transition from regular to chaotic dynamics of the investigated system are presented and discussed.

5. It has been shown that although the system is transversally loaded by sign-changeable load, a stiff stability system loss is observed during a transition from regular to chaotic regimes.

6. An increase of the impacting body velocity implies a transition from beam longitudinal to transversal vibrations.

7. The application of multi-layered beam systems allows us to control regular and chaotic system dynamics for both applied mathematical models.

8. Vibration type charts regarding two control parameters $\{q_0, \omega_p\}$ for different models and boundary conditions are constructed.

9. The influence of transversal shear effects and rotation inertia implies essential changes of the beam dynamics.

References

[1] S.A. Ambartsumian. General Theory of Anisotropic Shells, 1974.

[2] J. Awrejcewicz and V.A. Krysko. Nonclassical Thermoelastic Problems in Nonlinear Dynamics of Shells. Springer Verlag, Berlin, 2003.

[3] J. Awrejcewicz, V.A. Krysko, and I.V. Kravtsova. Mathematical Problems in Engineering. dynamics and statics of flexible axially-symmetric shallow shells, 2006. (DOI: 10.1155/MPE/2006/35672).

[4] J. Awrejcewicz, V.A. Krysko, and A.V. Krysko. Thermo-Dynamics of Plates and Shells. Springer Verlag, Berlin, 2007.

[5] J. Awrejcewicz, V.A. Krysko, and T.V. Shchekaturova. Transitions from regular to chaotic vibrations of spherical and conical axially-symmetric shells. International Journal of Structural Stability and Dynamics, 5(3):359–385, 2005.

[6] J. Awrejcewicz, V.A. Krysko, and A. Vakakis. Nonlinear Dynamics of Continuous Elastic Systems. Springer Verlag, Berlin, 2004.

[7] L. Azrar. Applications to large amplitude vibrations of beams and plates. PhD thesis, Ecole Mohammadia d'Ingenieurs Rabat, Morocco, 1999.

[8] L. Azrar, R. Benamar, and R.G. White. A semi-analytical approach to non-linear dynamic response problem of s-s and c-c beams at large vibration amplitudes Part I: General theory and application to the single mode approach to free and forced vibration analysis. Journal of Sound and Vibration, No.224:183–207, 1999.

[9] V.A. Krysko, M.V. Zhigalov, O.A. Saltykova, and A.S. Desiatova. Dissipative dynamics of geometrically nonlinear Bernoulli-Euler beams. (to appear).

[10] Han Qiang and Zheng Xiangfeng. Chaotic response of a large deflection beam and effect of the second order mode. European Journal of Mechanics, A 24(No. 6):944–956, 2005.

[11] P. Ribeiro. Non-linear forced vibrations of thin/thick beams and plates by the finite element and shooting methods. Computations and Structures, Vol. 82(No. 17-19):1413–1423, 2004.

[12] W. Szemplinska-Stupnicka. Non-linear normal modes and the generalized Ritz method in the problems of vibrations of non-linear elastic continuous systems. International Journal of Non-linear Mechanics, No. 18:149–165, 1983.

[13] A.S. Volmir. Nonlinear Dynamics of Plates and Shells, Nauka, Moscow, 1972. In Russian.

[14] Zhang Wei, Wang Fengxia, and Yao Minghui. Global bifurcations and chaotic dynamics in nonlinear non-planar oscillations of a parametrically excited cantilever beam. Nonlinear Dynamics, 40(No. 3):251–279, 2005.